Research Square

Preprints are preliminary reports that have not undergone peer review.
They should not be considered conclusive, used to inform clinical practice,
or referenced by the media as validated information.

Phase Separation of the E3 Ubiquitin Ligase OsRING20 Drives Antiviral Resistance in Rice through Targeted Ubiquitination of Viral Capsid Proteins

Chao Zhang

chaozhang21@126.com

Henan Agricultural University

Meirong Xiang

Henan Agricultural University

Pengyue Wang

Henan Agricultural University

Panpan Zhang

Edgene Biotechnology Co., Ltd.

Xinxin Jing

Henan Agricultural University https://orcid.org/0000-0002-6464-3318

Huiting Xie

Fujian Agriculture and Forestry University

Zhenlu Zhang

Shandong Agricultural University

Bixia Qin

Guangxi Academy of Agricultural Sciences

Fang Duan

Edgene Biotechnology Co., Ltd.

Chaonan Wang

College of Plant Protection, Henan Agricultural University

Zhanbiao Li

South China Agricultural University

honglian li

Henan Agricultural University

Zujian Wu

Fujian Agricultural and Forest University

Pengbai Li

Henan Agricultural University

Article

Keywords:

Posted Date: November 17th, 2026

DOI: https://doi.org/10.21203/rs.3.rs-11465987/v1

License: This work is licensed under a Creative Commons Attribution 4.0 International License.
Read Full License

Additional Declarations: There is **NO** Competing Interest.

Phase Separation of the E3 Ubiquitin Ligase OsRING20 Drives Antiviral Resistance in Rice through Targeted Ubiquitination of Viral Capsid Proteins

Meirong Xiang[1,#], Pengyue Wang[1,2,#], Panpan Zhang[3], Xinxin Jing[4], Huiting Xie[5], Zhenlu Zhang[6], Bixia Qin[5], Fang Duan[3], Chaonan Wang[1], Zhanbiao Li[5], Honglian Li[1], Zujian Wu[2], Pengbai Li[1,*], Chao Zhang[1,*]

[1]The Engineering Research Center for Plant Health Protection Technology in Henan Province, College of Plant Protection, Henan Agricultural University, Zhengzhou, 450002, China.
[2]State Key Laboratory of Agricultural and Forestry Biosecurity, College of Plant Protection, Fujian Agriculture and Forestry University, Fuzhou 350002, China.
[3]Edgene Biotechnology Co., Ltd. Wuhan, 430206, China.
[4]Institute of Plant Protection, Henan Academy of Agricultural Sciences, Zhengzhou, Henan 450002, China.
[5]Plant Protection Research Institute, Guangxi Academy of Agricultural Sciences, Guangxi Key Laboratory of Biology for Crop Diseases and Insect Pests, Key Laboratory of Green Prevention and Control on Fruits and Vegetables in South China, Ministry of Agriculture and Rural Affairs, Nanning 530007, China.
[6]State Key Laboratory of Crop Biology, College of Horticulture Science and Engineering, Shandong Agricultural University, Tai'an 271000, China.

[#]These authors contributed equally to this work.

[*]Correspondences: chaozhang21@126.com; lipengbai930409@163.com.

ABSTRACT

E3 ubiquitin ligases are pivotal regulators of plant immunity and promising targets for engineering pathogen-resistant crops. Here, we identify OsRING20, a rice RING-type E3 ubiquitin ligase that forms homodimers through its RING domain, and targets the capsid proteins (P10) of rice black-streak dwarf virus (RBSDV) for degradation via the ubiquitin-proteasome system. We further identified Lys363 and Lys555 within the RBSDV P10 as the primary ubiquitination sites for OsRING20. Notably, OsRING20 undergoes liquid-liquid phase separation (LLPS) through its N-terminal intrinsically disordered region (IDR1), forming biomolecular condensates that act as a degradation hub for viral P10. This process is critically regulated by serine residues Ser45/46 in IDR1. Cellular and biochemical evidence indicates that P10 remodels the oligomeric

status of OsRING20, promoting its dimerization and subsequent LLPS. Overexpression of *OsRING20* confers strong resistance against both RBSDV and southern rice black-streaked dwarf virus (SRBSDV) without compromising normal vegetative growth. Our findings demonstrate that phase separation-regulated E3 ligase condensates are central to plant antiviral immunity. This provides a novel theoretical mechanistic insight for understanding disease resistance and offers key molecular targets for resistance breeding.

INTRODUCTION

Ubiquitination, a crucial post-translational modification, serves as a central regulatory mechanism in the ubiquitin-proteasome system (UPS) that governs diverse biological processes including the growth traits and stress responses in plants (1-3). This process involves a well-characterized enzymatic cascade comprising ubiquitin activating enzyme (E1), ubiquitin-conjugating enzyme (E2), and ubiquitin ligase (E3), with E3 ligases determining substrate specificity (4). Following ubiquitination, target proteins are recognized and degraded by the 26S proteasome. Plant E3 ubiquitin ligases are categorized into four main classes based on their structural domains and substrate recognition mechanisms: Homologous to E6-AP Carboxyl Terminus (HECT), Really Interesting New Gene (RING), U-box, and Cullin (Cul)-RING ligases (CRLs) (5-7). Among these, RING-domain E3 ubiquitin ligases represent the most abundant family in plants, characterized by their canonical RING finger domain that facilitates direct transfer of ubiquitin from E2 enzymes to substrate lysine residues (8, 9). Emerging evidence highlights the dual roles of RING-type E3 ligases in plant-virus infections, in which they can be hijacked by viruses to promote infection or employed by plants as antiviral defense components (10, 11). As one of the simplest pathogenic agents in plants, viruses often utilize or manipulate the functions of RING E3 ubiquitin ligases to promote their own infection. For example, geminivirus infection induces a RING domain-containing E3 ubiquitin ligase to epigenetically promote the transcription of the viral proteins C2 and C3 (12). A RING ligase-mediated polyubiquitination of rice stripe virus NS3 regulates its nuclear translocation, enhancing viral replication

through miRNA-induced fibrillin 2 upregulation (13). RBSDV-encoded P6 impairs rice antiviral defense by promoting OsSCE1b ubiquitination and degradation, thereby inhibiting the OsPelota-mediated antiviral RNA decay pathway (14). Additionally, an m^6A methyltransferase positively regulates rice antiviral resistance via ubiquitination-dependent viral protein degradation, offering a promising target for crop disease resistance molecular breeding (15). On the contrary, viral proteins can be directly targeted by RING E3 ligases for degradation. The RING finger domain-containing E3 ligase HRD1 enhances plant antiviral immunity by targeting viral movement proteins for degradation (16). A recent study uncovers a novel antiviral resistance strategy in rice plants, in which RING1-IBR-RING2 E3 ligase perceives viral infections and initiates antiviral responses through activating jasmonic acid (JA)-mediated immunity pathway (17). Furthermore, the crosstalk between JA and brassinosteroid (BR) signaling is finely modulated by key kinase-JAZ module in rice. The OsGSK2 kinase has been demonstrated to integrate BR and JA signaling pathways via physical interaction with OsJAZ4, providing an underlying molecular basis for the coordination of hormone-mediated immune responses in rice (18). These findings elucidate the sophisticated defense-counter-defense dynamics involving RING E3 ligases between plants and viruses.

Liquid-liquid phase separation (LLPS) is ubiquitous in physics and materials science (19). In recent years, LLPS has entered the field of plant biology, often related to plant growth, development and stress response (20-23). Emerging evidence highlights its significance in plant-virus interaction systems (24, 25). On one hand, plants exploit LLPS to form condensates that compartmentalize viral factories, as demonstrated by the sequestration of cauliflower mosaic virus (CaMV) replication complexes, thereby inhibiting virus infection (26). Conversely, viruses hijack LLPS to create viral replication hubs that enhance viral genome replication, systemic movement or evasion of host immunity. In *Arabidopsis*, host RNA helicases facilitate the formation of viral bodies via promoting the phase separation of turnip mosaic virus (TuMV) VPg proteins, thereby enhancing virus proliferation (27). Pea enation

mosaic virus 2 (PEMV2) movement protein p26 undergoes phase separation with cytoskeletal components or disrupts ribosome assembly and translation to aid specific stages of viral replication (28, 29). Barley yellow striate mosaic virus (BYSMV) phosphoprotein (P) forms condensates that promote viroplasm formation and virus replication, with host casein kinase 1 (CK1) inhibiting this process to restrict virus infection (30). We recently determined that rice grassy stunt virus (RGSV) P1 protein recruits OsCIPK23 into nuclear condensates with coilin to promote systemic infection (31), pointing to an involvement of cajal bodies (CBs), the membraneless organelles formed through LLPS in the nucleus, during virus infection in rice. In addition, phosphoprotein condensates of plant negative-strand RNA viruses hijack host membrane trafficking and lipid biosynthesis to establish viral replication factories, uncovering the assembly mechanism of virus-induced phase-separated condensates (32). Meanwhile, viral proteins enhance OsTSN1's RNA decay activity via phase separation and multimerization, suppressing rice antiviral defense and revealing a novel phase separation-mediated mechanism for viral hijacking of host RNA metabolism (33). These findings collectively demonstrate that LLPS serves as a key battleground in plant-virus co-evolution. However, current knowledge of virus-host interactions occurring through LLPS particularly regarding plant viruses is still limited.

While extensive research has elucidated conserved roles of E3 ubiquitin ligases and LLPS in plant-virus interactions, the role of LLPS in E3-mediated protein degradation remains largely unexplored. Current models of E3-mediated substrate degradation during viral infection rely primarily on biochemical evidence, lacking spatiotemporal resolution of these processes at the cellular level. Notably, multiple RING-type E3 ligases exhibit phase separation capability, yet it remains unclear whether they self-assemble into condensates or recruit substrate proteins into phase-separated droplets to facilitate ubiquitination. This knowledge gap likely stems from the inherently transient nature of E3-substrate interactions, which challenges conventional detection methods.

Rice black-streaked dwarf virus disease, caused by RBSDV, a member of the *Fijivirus* genus in the *Reoviridae* family, and transmitted persistently by the small brown planthopper (*Laodelphax striatellus*, SBPH), is a devastating viral disease severely threatening global rice and maize production (34, 35). The virus forms 75-80 nm icosahedral two-layered virions and harbors a genome of ten double-stranded RNA segments (S1-S10) responsible for viral structure, replication, and pathogenicity (34). Genomic variation and selection pressure differ across RBSDV segments, with the highly conserved S10 segment encoding the outer capsid protein P10, a key factor participating in viral pathogenicity and host interaction (36). Here, we characterize OsRING20, a RING-type E3 ubiquitin ligase that undergoes LLPS and directly interacts with the P10, the capsid protein of RBSDV. This interaction targets P10 for polyubiquitin-mediated degradation via the 26S proteasome. The RING domain of OsRING20 mediates critical self-interactions necessary for P10 targeting. Additionally, we identify Lys363 and Lys555 as the primary ubiquitination sites within the P10. We demonstrate that Ser45 and Ser46 residues are essential for OsRING20's phase separation properties, which are directly linked to its E3 ligase activity and subsequent viral P10 degradation. Cellular and biochemical evidence also illustrates that P10 itself modulates the phase separation behavior of OsRING20. Genetic analyses confirm that OsRING20 positively regulates rice defense against RBSDV, and also mediates the degradation of SP10, the capsid protein of southern rice black-streaked dwarf virus (SRBSDV). Given the high sequence conservation of capsid proteins between RBSDV and SRBSDV, indicating OsRING20 exhibits conserved resistance against *Fijivirus* members. Collectively, our findings provide the first cellular evidence connecting LLPS with ubiquitin-proteasome system function in plant immunity and establish OsRING20 as a promising target for engineering virus-resistant rice varieties without compromising normal vegetative growth.

RESULTS

OsRING20 physically interacts with the capsid protein P10 of RBSDV

To investigate UPS-mediated antiviral defenses against fijiviruses, we performed a

yeast two-hybrid screen of a rice cDNA library using RBSDV capsid protein P10 as bait, identifying OsRING20, a RING-type E3 ubiquitin ligase, as a direct interactor. Sequence alignment using the MEGA7.0 software revealed that OsRING20 contains a conserved RING finger domain, a hallmark feature of E3 ubiquitin ligases, indicating that it belongs to the RING H2-type E3 ubiquitin ligase family (Fig. S1). Meanwhile, RBSDV infection did not significantly alter the transcript levels of OsRING20 (Fig. S2). Computational structural modeling predicted the binding interface between OsRING20 and P10 (Fig. 1A), which was consistently validated across multiple assays. Yeast two-hybrid (Y2H) assays verified the strong interaction between the two proteins under stringent screening conditions, and the α-galactosidase (X-gal) staining assay was further performed to rule out false positives (Fig. 1B). Bimolecular fluorescence complementation assays (BiFC) in *N. benthamiana* revealed reconstituted YFP fluorescence from OsRING20-nYFP/P10-cYFP pairs in nuclear puncta (Fig. 1C). Furthermore, co-immunoprecipitation *in planta* confirmed that Flag-tagged P10 co-precipitates with GFP-labeled OsRING20, but not with control GFP (Fig. 1D). *In vitro* pull-down assays demonstrated specific physical binding between MBP-fused P10 and GST-fused OsRING20 (Fig. 1E). Additionally, Y2H screening revealed that OsRING20 did not interact with other RBSDV-encoded proteins (Fig. S3). Collectively, these results establish a specific and physiologically relevant interaction between OsRING20 and P10, implicating OsRING20 in UPS-mediated antiviral responses.

OsRING20 targets P10 for degradation through UPS-dependent pathway

In vitro and *in vivo* ubiquitination assays confirmed that OsRING20 directly catalyzes the polyubiquitination of P10 (Fig. 2A and Fig. S4A). *In planta* degradation assays determined that OsRING20 promotes P10 degradation, and this effect that was abolished by the proteasome inhibitor MG132, indicating that OsRING20 targets P10 for degradation via the ubiquitin-proteasome system (UPS) (Fig. 2B). This process was further shown to be dose-dependent, as evidenced by the progressive reduction of P10 levels with increasing OsRING20 expression (Fig. S4B). To substantiate these in a rice cell-free system, we performed a degradation assay using protein extracts from

ZH11, *OsRING20*- overexpressing, and *OsRING20*-knockout rice seedlings. Initial levels of purified GST-fused P10 protein equivalent across all reactions. Upon incubation, the results showed that GST-P10 protein was gradually degraded in the cell-free degradation buffer prepared from ZH11 samples as incubation time was extended (Fig. 2C and Fig. S4C). Notably, the degradation rate of GST-P10 was significantly higher in *OsRING20*-OE samples compared to ZH11 samples. Conversely, GST-P10 was not degraded in the *OsRING20*-KO cell-free degradation buffer. Additionally, GST-P10 degradation was inhibited by MG132 treatment. GST protein was used as a control, and results demonstrated that OsRING20 did not cause the degradation of GST protein (Fig. 2C). Together, these findings establish that OsRING20 targets P10 for degradation in a UPS-dependent manner.

The RING finger domain is essential for E3 ubiquitin ligase activity. Structural modeling of OsRING20 suggested a capacity for homodimerization (Fig. 3A). To investigate the role of its RING domain in substrate targeting, we generated a RING domain deletion mutant (Fig. 3B). Y2H and BiFC assays consistently revealed that while robust self-interact strictly requires the RING domain, deletion of this region does not disrupt binding to the P10 protein (Fig. 3C-D). Despite retaining P10 interaction, the deletion mutant was unable to ubiquitinate P10, underscoring that an intact RING domain is indispensable for catalytic E3 ligase activity (Fig. 3E). Consequently, this mutant also failed to promote P10 degradation (Fig. 3F). To further dissect the catalytic mechanism, we generated a double-site mutant, OsRING20$^{C529A/H531A}$, targeting conserved residues within the canonical RING motif (Fig. S5A-B). This mutant maintained nuclear localization and retained the ability to self-interaction and bind P10 (Fig. S5C-E). Notably, however, it formed significantly smaller nuclear puncta than the wild-type OsRING20 protein (Fig. S5C) and lost its ability to degrade P10 *in planta* (Fig. S5F). These results demonstrate that RING domain of OsRING20 is essential for mediating the degradation of the viral P10 protein. Collectively, our findings establish OsRING20 as a modular E3 ubiquitin ligase that oligomerizes through its RING domain to ubiquitinate P10 and facilitate its

UPS-dependent degradation, revealing a targeted antiviral mechanism in rice.

OsRING20 specifically ubiquitinates P10 at lysine residues 363 and 555

Through UbPred bioinformatics analysis (37), it was found that P10 has five putative ubiquitination sites. Among them, K363 and K555 are the highly likely ubiquitination sites in P10 (Fig. 4A), and mutations at these five potential ubiquitination sites on the P10 protein do not affect its subcellular localization (Fig. S6). We further performed protein degradation assays of these five P10 single-site mutants and found that only the K363 and K555A mutations markedly attenuated OsRING20-mediated P10 degradation (Fig. S7). Therefore, we generated a double sites mutation of P10 at lysine residues 363 and 555 (P10-K363/555A). Y2H, BiFC, Co-IP, and pull down assays showed that lysine residues 363 and 555 of P10 are not essential for OsRING20 recognition (Fig. 4B-E). *In planta* degradation assays demonstrated the P10-K363/555A mutant resisted OsRING20-mediated ubiquitination and degradation (Fig. 4F-G). Crucially, these results precisely map the molecular determinants of OsRING20's substrate ubiquitination modification and degradation.

OsRING20 forms nuclear biomolecular condensates via LLPS

Confocal microscopy confirmed the nuclear localization of OsRING20 in plant cells (Fig. 5A). Consistent with observations in *N. benthamiana*, YFP-OsRING20 also formed nuclear liquid-like condensates in rice protoplasts (Fig. S8A). OsRING20 exhibited two distinct nuclear distribution patterns: Type I formed diffuse aggregation without obvious condensate formation and weak phase-separation activity (~60% of cells), whereas Type II showed well-defined spherical condensates with robust LLPS propensity (~40% of cells) (Fig. 5B). Bioinformatics analysis using PONDR identified two intrinsically disordered regions (IDR1 and IDR2; Fig. 5C), a hallmark of LLPS-prone proteins. Fluorescence recovery after photobleaching (FRAP) assays *in planta* revealed dynamic recovery within condensates: full condensate bleaching showed gradual fluorescence recovery plateauing at ~90 s (Fig. 5D-E), while internal bleaching exhibited rapid, near-complete recovery within ~20 s (Fig. 5F-G), confirming liquid-like behavior. Recombinant YFP-labeled YFP-OsRING20 purified

from *Escherichia coli* (Fig. 5H-I) formed dynamic condensates under 500 mM NaCl treatment (Fig. 5J), with significant fluorescence recovery in FRAP experiments (Fig. 5K-L), validating LLPS *in vitro*. We further tested a NaCl concentration gradient and found that increasing ionic strength progressively enhances the LLPS propensity of purified His-YFP-OsRING20, revealing that elevated NaCl promotes OsRING20 condensate assembly (Fig. S8B). Furthermore, OsRING20 condensates underwent spontaneous fusion and fission *in vivo* (Fig. 5M), demonstrating classical liquid-phase dynamics. Collectively, these data establish OsRING20 as a phase-separating protein and propose its role as a nuclear biomolecular condensate hub for antiviral ubiquitination.

IDR1 is a key domain that mediates the phase separation of OsRING20 and facilitates P10 protein degradation

To identify key domains regulating LLPS in OsRING20, we generated truncation mutants targeting its two intrinsically disordered regions (IDR1, IDR2) and the RING domain (Fig. 6A). Confocal microscopy revealed that deletion of IDR1 (dIDR1) drastically reduced nuclear condensate formation, while dIDR2 and dRING mutants retained nuclear punctate structures (Fig. 6B), indicating IDR1 is essential for LLPS. FRAP assays confirmed severely impaired dynamics in dIDR1, whereas dIDR2 and dRING exhibited wild-type-like recovery (Fig. 6C-D). Given the regulatory role of phosphorylation in IDRs (38), we generated six serine-to-alanine mutants within IDR1 (Fig. S9A). The S45/46A double mutant exhibited diffuse nuclear localization and loss of nuclear condensates (Fig. 6E and Fig. S9B), with significantly reduced mobility in FRAP experiments (Fig. 6F-G). Conversely, the phosphomimetic S45/46D mutant retained typical LLPS capability (Fig. S10A-C). *In vitro* reconstitution using purified proteins showed that wild-type OsRING20 formed abundant condensates under 500 mM NaCl, enlarging at higher salt concentrations. In contrast, dIDR1 and S45/46A mutants formed few and smaller condensates only at 1000 mM NaCl (Fig. S11). These results identify IDR1 as the central driver of OsRING20 LLPS and underscore Ser45/Ser46 as critical residues governing its phase behavior, providing mechanistic

insight into the formation and regulation of antiviral biomolecular condensates.

BiFC assays confirmed that LLPS-deficient mutants (dIDR1 and S45/46A) retained self-interaction and P10 binding (Fig. S12), but both failed to promote P10 degradation *in planta* (Fig. 6H-I), indicating that phase separation is essential for ubiquitination activity rather than substrate recognition and binding. Collectively, these results demonstrate that LLPS of OsRING20 is required for its E3 ligase function in mediating targeted P10 degradation, revealing a mechanistic link between biomolecular condensation and antiviral ubiquitination.

P10 as an enhancer of the phase separation of OsRING20

To examine whether the P10 protein promotes the phase separation of OsRING20, we co-expressed YFP-OsRING20 with either P10-Flag or GUS-Flag in *N. benthamiana* leaves. Confocal microscopy and quantitative analysis showed a significantly higher proportion of cells containing OsRING20 Type II when co-expressed with P10-Flag compared to GUS-Flag controls (Fig. 7A-B), despite comparable YFP-OsRING20 expression levels (Fig. 7C). *In vitro,* GST-P10, but not GST alone, efficiently promoted His-YFP-OsRING20 condensate formation under both basal and 800 mM NaCl conditions (Fig. 7D-E). Purified proteins were verified through western blot using anti-GFP or anti-GST antibodies (Fig. 7F). Based on the above results, we hypothesized that P10 promotes OsRING20 phase separation. To test this, we first treated purified His-YFP-OsRING20 with a NaCl concentration gradient and performed native PAGE analysis. Immunoblotting revealed that the abundance of OsRING20 dimers increased progressively with elevated ionic strength (Fig. 7G-H). We further assessed the effect of GST-P10 on His-YFP-OsRING20, and found that GST-P10 promoted a relative increase in the dimeric fraction of OsRING20 compared to the GST control (Fig. 7I). Consistent with the *in vivo* confocal observations, the proportion of cells exhibiting Type II OsRING20 with high liquid-like LLPS mobility was markedly increased in the presence of P10. Together, these results demonstrate that P10 acts as an enhancer of OsRING20 phase separation.

OsRING20 improves resistance to RBSDV without causing obvious vegetative

growth defects in rice

To elucidate the antiviral role of OsRING20, we generated overexpression (*OsRING20* OE) and knockout (*OsRING20* KO) transgenic rice lines. Overexpression lines showed no significant growth defects were observed during the vegetative growth stage (Fig. 8A-D and S13) but exhibited strong resistance to RBSDV, with markedly reduced symptoms and viral RNA levels (*P4*, *P8*, *P10*; Fig. 8E-F). Conversely, *OsRING20* knockout mutants displayed enhanced susceptibility and elevated viral accumulation.

To determine whether the phase separation of OsRING20 governs its E3 ubiquitin ligase activity and antiviral function, we performed genetic complementation assays in an *OsRING20*-knockout background using constructs expressing *YFP-OsRING20*, three mutants including *YFP-OsRING20-dIDR1*, *YFP-OsRING20-S45/46A*, and *YFP-OsRING20-dRING* (Fig. S14A-B). Confocal imaging of rice protoplasts from each complemented line confirmed that only YFP-OsRING20 and YFP-OsRING20-dRING formed liquid condensates, while dIDR1 and S45/46A mutants showed diffuse nuclear localization (Fig. S14C), reinforcing the role of IDR1 and Ser45/46 in LLPS regulation of OsRING20. Upon RBSDV challenge, *YFP-OsRING20*-complemented lines exhibited visible resistance compared to *OsRING20*-knockout lines, marked by reduced symptoms and diminished viral accumulation, whereas the *YFP-OsRING20-dIDR1*, *YFP-OsRING20-S45/46A*, and *YFP-OsRING20-dRING* complemented lines remained susceptible, phenocopying non-complemented mutants (Fig. 8G-H). Together, these results demonstrate that IDR1-mediated phase separation is essential for OsRING20's E3 activity and antiviral function, establishing LLPS of OsRING20 as the mechanistic basis for resistance.

OsRING20 confers resistance by targeting SRBSDV capsid proteins

Given the high sequence conservation between the capsid proteins of RBSDV and southern SRBSDV (Fig. S15), we examined whether OsRING20 also targets SRBSDV capsid protein (SP10). Structural modeling predicted a conserved binding mode (Fig. 9A), validated by BiFC and pull-down assays (Fig. 9B-C). Subsequently, we confirmed that OsRING20 mediates SP10 degradation both *in planta* and *in vitro* (Fig.

9D-E and Fig. S16A). Upon SRBSDV challenge via *Sogatella furcifera*, OsRING20 overexpressing lines exhibited strong resistance with reduced viral accumulation (Fig. 9F-I), whereas knockout mutants were highly susceptible. Similarly, YFP-OsRING20-complemented lines compensates for the resistance loss of the *OsRING20*-knockout plants, while *YFP-OsRING20-dIDR1*, *YFP-OsRING20-S45/46A*, and *YFP-OsRING20-dRING* complemented lines remained susceptible (Fig. S16B-C). Collectively, these results demonstrate that OsRING20 confers resistance against RBSDV and SRBSDV through a conserved mechanism of P10/SP10 degradation, without compromising normal vegetative growth. This positions OsRING20 as promising and durable genetic resource for breeding virus-resistant rice.

DISCUSSION

Our study establishes OsRING20 as a positive regulator of rice antiviral defense against fijiviruses. Crucially, we provide compelling evidence that the E3 ligase activity of OsRING20, required for the polyubiquitin-mediated degradation of viral coat proteins, is mechanistically dependent on its ability to undergo LLPS (Fig. 10).

The E3 ligase-mediated polyubiquitination and degradation of target substrates represents a conserved regulatory mechanism for immune responses across eukaryotes (39-41). In both plant and animal viral infections, E3 ligases can directly target viral proteins for proteasomal degradation, thereby suppressing viral propagation (40, 42). For instance, the tobacco RING E3 ligase NtRFP1 recognizes and ubiquitinates the βC1 protein encoded by the betasatellite of tomato yellow leaf curl China virus, leading to its proteasomal degradation and disease symptom alleviation (43). In rice, the RING-H2 finger E3 ligase OsRFPH2-10 facilitates polyubiquitination and degradation of the rice dwarf virus P2 protein, contributing to antiviral defense during early infection (44). Moreover, UBL5 proteins in rice and *N. benthamiana* destabilize the P3 protein of rice stripe virus (RSV) through the proteasomal pathway, conferring resistance to RSV (45). In animals, the E3 ligase TRIM22 restricts SARS-CoV-2 replication by promoting proteasomal degradation of viral NSP8 (46). In this study, we demonstrate that OsRING20 acts as a RING-type E3 ubiquitin ligase that directly

interacts with the coat proteins of fijiviruses, promoting their polyubiquitination and subsequent degradation via the 26S proteasome. Genetic evidence confirms that OsRING20 positively regulates resistance against both RBSDV and SRBSDV. Notably, E3 ubiquitin ligases typically possess multiple substrates, and OsRING20 may simultaneously target viral proteins and certain host negative regulators of immunity, thereby synergistically enhancing antiviral defense through the degradation of both. Future identification of its full substrate spectrum will provide a more comprehensive understanding of its antiviral mechanism. Collectively, these findings underscore the ubiquitin-proteasome system, orchestrated by an E3 ligase, as a conserved antiviral strategy that operates by targeting key viral proteins for degradation.

LLPS drives the formation of membraneless organelles that serve critical roles in diverse cellular processes (47). Recent advances in characterizing LLPS, both *in vitro* and *in vivo*, have provided new insights into its roles in contexts ranging from growth and development to disease responses (48, 49). Notably, emerging evidence implicates ubiquitin-associated molecules involving biomolecular condensates formed through LLPS (48). In yeast, LLPS of Lge1, a protein essential for H2B monoubiquitination, directly stimulates the histone ubiquitination specifically across gene bodies, demonstrating that phase separation directs ubiquitination process (50). In plants, *Arabidopsis* NPR1 forms cytoplasmic condensates that facilitate the assembly of functional NPR1-CRL3 complexes, which regulate plant immunity through UPS by targeting immune regulators such as EDS1 and WRKY transcription factors for degradation (51). As obligate intracellular parasites, viruses extensively manipulate host LLPS and ubiquitination systems to promote their propagation or evade immune defenses (52). Recent advances have deepened our mechanistic understanding of LLPS-mediated plant-virus interactions. Lin and Nagy (2024) demonstrated that a positive-strand RNA virus hijacks host cytosolic proteins to form condensate substructures within membranous replication organelles, exposing a novel spatial regulatory mechanism that sustains viral replication (53). Similarly, Zou *et al*. (54)

reported that a bunyavirus protein disrupts SERRATE phase separation, impairing microRNA biogenesis to enhance viral pathogenicity. In contrast, engineered biomolecular condensates are capable of limiting tobacco mosaic virus (TMV) accumulation and alleviating disease symptoms (55), highlighting that artificial LLPS modulation is a promising strategy for developing antiviral approaches. While E3 ubiquitin ligases are known to play dual roles in plant-virus interactions, cellular-level evidence linking LLPS to their regulatory mechanisms during viral infection remains scarce. Our study establishes that LLPS is indispensable for OsRING20 E3 ligase activity, as evidenced by the findings that disruption of OsRING20 phase separation impaired its ability to ubiquitinate and degrade the P10. Notably, the observation that P10 promotes OsRING20 phase separation suggests a positive feedback mechanism in host antiviral defense: P10-induced OsRING20 LLPS further enhances the ubiquitination and degradation efficiency of viral capsid proteins, thereby restricting viral proliferation and systemic infection. This finding enriches the mechanistic understanding of how plants leverage phase separation to combat viral pathogens.

Many proteins that drive intracellular phase separation contain intrinsically disordered regions (IDRs), which are characterized by low-complexity, repetitive amino acid sequences that favor conformational heterogeneity over stable folded structures (56, 57). Post-translational modifications, such as phosphorylation can finely regulate the phase behavior of IDRs (58). For instance, phosphorylation of the central IDR of the barley yellow striate mosaic virus P protein by the host protein CK1 suppresses its phase separation (30). Our study further revealed that Ser45 and Ser46 within the IDR1 of OsRING20 are essential for its phase separation, and their mutation compromises viral CPs degradation. This implies that phosphorylation at these residues is critical for OsRING20's phase separation ability, which in turn is essential for its E3 ligase capacity and the subsequent degradation of viral CPs. However, the specific kinase responsible for phosphorylating these residues remains to be identified. Future identification of this kinase will help elucidate the upstream regulatory mechanism of OsRING20 phase separation. Additionally, the precise

410 physicochemical mechanism by which LLPS enhances the E3 ligase activity of
411 OsRING20 warrants further investigation, and systematic screening for potential host
412 substrates of OsRING20 under virus-infected conditions will provide a more
413 comprehensive understanding of its antiviral function.

414 In plants, disease management strategies that target functional E3 ubiquitin ligases
415 have gained significant attention. The rice genome encodes over 1000 putative E3
416 ligases (59), and numerous studies over the past two decades have identified specific
417 E3s as crucial modulators of rice immunity (60), making them valuable targets for
418 breeding disease-resistant cultivars (61). Most characterized rice RING-type E3
419 ligases, such as OsRING113 and the microtubule-associated C4HC3-type RING E3
420 ligase (MEL), act as positive regulators, boosting broad-spectrum immunity through
421 mechanisms like MAPK activation, reactive oxygen species (ROS) bursts, and
422 transcriptional induction of defense-related genes (62, 63). Conversely, other
423 RING-type E3 ligases like OsRFPH2-6, OsREIW1, and OsATL32 serve as negative
424 regulators of defense (64-67). This duality has spurred the use of transgenic and
425 gene-editing approaches to either activate immune-promoting E3 ligases or suppress
426 negative regulators, enabling the development of stably resistant varieties. With limited
427 availability of effective biochemical pesticides, breeding resistant cultivars offers an
428 economical and sustainable solution for viral disease management (68), and
429 immune-related E3 ligase genes are particularly promising for engineering antiviral
430 crops (61). Our study demonstrates that OsRING20 enhances rice resistance to
431 fijiviruses without causing significant growth defects during the vegetative growth
432 stage, underscoring its potential for breeding programs aimed at antiviral resistance.
433 However, the intricate interplay between plant viruses and their insect vectors
434 complicates disease management. For example, plant viruses attract insect vectors by
435 encoding host-mimicking proteins, thereby promoting their transmission and inducing
436 disease symptoms, which reveals a novel host mimicry strategy for viral transmission
437 and pathogenesis (69). Furthermore, plant defense responses that restrict viral
438 movement in the phloem can paradoxically enhance vector transmission efficiency,

highlighting a trade-off between plant defense and viral spread (70). These insights highlight the need for holistic disease management strategies that consider the dynamic tripartite interactions between the virus, host, and vector.

Given their crucial role in modulating both host and viral proteins, E3 ubiquitin ligases have emerged as promising therapeutic targets for combating viral infections (71). While significant progress has been made in mammalian systems, with candidates advancing to preclinical and clinical stages, plant science has also witnessed breakthroughs (66). Notably, Zhao *et al*. (72) recently identified a U-box E3 ubiquitin ligase involved in natural defense against Huanglongbing (HLB). HLB is a devastating vector-borne citrus disease caused by *Candidatus* Liberibacter asiaticus (*C*Las). The researchers further developed an AI-assisted screening platform to discover antiproteolytic peptides targeting PUB21 E3 ligase activity. One such peptide, APP3-14, demonstrated significant efficacy in inhibiting cLas colonization and spread, providing a paradigm for E3-targeted disease management in plants (73). Therefore, elucidating the detailed regulatory mechanisms of E3 ligases in disease pathogenesis remains a critical reseach priority. Such studies are fundamental for developing effective disease control strategies, whether through targeted resistance breeding programs or precision therapeutic development.

METHOD AND MATERIALS

Plant growth and virus inoculation

Wild-type (*Oryza sativa* cv. Zhonghua11) and transgenic rice plants were maintained in a greenhouse at 28-30°C under a 16 hour (h) light/8 h dark photoperiod. *N. benthamiana* plants were grown in controlled climate chambers at 25°C under a 16 h light/8 h dark cycle. For viral challenges, RBSDV inoculations were performed using viruliferous leafhoppers (*Laodelphax striatellus*), while SRBSDV inoculations were performed using viruliferous leafhoppers (*Sogatella furcifera*) following established protocols. All infection assays were conducted with at least three independent biological replicates.

Yeast two-hybrid (Y2H) assay

Y2H analysis was performed using the Matchmaker Gold Yeast Two-Hybrid System (Clontech) according to the manufacturer's protocol. The bait construct BD-P10 and prey construct AD-OsRING20 were co-transformed into yeast strain Y2HGold using the lithium acetate method. Transformants were selected on synthetic defined medium lacking leucine and tryptophan (SD/-Leu/-Trp) and incubated at 30°C for 72 h.

For interaction testing, positive colonies were serially diluted (10^{-1} to 10^{-4}) in sterile water and spotted onto high-stringency selection medium (SD/-Leu/-Trp/-His/-Ade). The resulting interactions were further validated using a α-galactosidase (X-gal) assay. All protein-protein interactions were assessed after 72 h incubation at 30°C.

Bimolecular fluorescence complementation (BiFC) assays

The recombinant plasmids P10-cYFP/P10-nYFP and OsRING20-nYFP/OsRING20-cYFP were individually transformed into *Agrobacterium tumefaciens* GV3101 and grown overnight in LB liquid medium containing rifampicin (50 μg/ml) and kanamycin (50 μg/ml). Bacterial cultures were pelleted by centrifugation, resuspended in inoculation buffer (10 mM $MgCl_2$, 100 mM MES, and 2 mM acetosyringone), and adjusted to OD_{600}=0.8-1.0. Equal volumes of the two Agrobacterium suspensions were combined, incubated at room temperature for 2-3 h, and then infiltrated into 4-6 week-old *N. benthamiana* leaves using needleless syringes. YFP fluorescence was examined by confocal microscopy at 2 days post-infiltration (dpi).

Co-immunoprecipitation (Co-IP) assays

The recombinant plasmids P10-Flag and YFP-OsRING20 were separately transformed into *Agrobacterium tumefaciens* strain GV3101. The agrobacterium strain containing P10-Flag was mixed in equal volumes with those containing YFP-OsRING20 and 35S-YFP, respectively, and co-inoculated onto *N. benthamiana* leaves. At 48 hpi, the inoculated leaves were collected, and total protein was extracted. The total protein samples were then incubated with anti-GFP agarose beads (Sigma) at 4°C for 3 h,

followed by five washes with PBS buffer. The input and co-immunoprecipitated protein samples were analyzed by Western blot using anti-GFP (clone 7G9, #M20004, Abmart, 1:5000) or anti-Flag (DYKDDDDK Tag, #0912-1, Huabio, 1:5000) antibody, and HRP-conjugated goat anti-Mouse IgG (#M21001, Abmart, 1:5000) was used as the secondary antibody for immunodetection.

Recombinant protein expression and purification

The plasmids pGEX-OsRING20 and pMAL-P10 were independently transformed into *E. coli* BL21(DE3) competent cells. Transformed colonies were selected on LB agar plates containing kanamycin (50 μg/mL) and cultured overnight at 37°C. For protein expression, single colonies were inoculated into 5 mL LB medium with kanamycin (50 μg/mL) and grown at 37°C with shaking (220 rpm) until the OD_{600} reached 0.6-0.8. Protein expression was induced by adding 0.3 mM IPTG (Sigma-Aldrich), followed by incubation for 10 h at 23°C with continuous shaking (150 rpm). Cells were harvested by centrifugation (4,000 × g, 10 min, 4°C) and resuspended in ice-cold lysis buffer (20 mM Tris-HCl pH 7.5, 500 mM NaCl, 10% glycerol, 1 mM PMSF). Cell lysis was performed by sonication (30% amplitude, 5 sec pulse/5 sec rest, 5 min total) on ice. The lysate was clarified by centrifugation (12,000 × g, 30 min, 4°C), and the supernatant was collected for protein purification. pGEX-OsRING20 and pMAL-P10 fusion proteins were affinity-purified using nickel-NTA and amylose affinity chromatography, respectively, following standard protocols. For subsequent functional analyses, a series of expression constructs were generated: OsRING20 and its mutant variants were cloned into the pET-28a vector for expression as His-tagged fusion proteins; wild-type P10 was cloned into a pGEX vector for expression as a GST-tagged fusion protein; and P10 mutants along with SP10 were cloned into the pMAL vector for expression as MBP-tagged fusion proteins. Following expression and initial purification using the standard protocols described above, the IPTG induction conditions, including concentration, temperature, and duration, were systematically optimized for each protein according to its individual expression characteristics and solubility profile, thereby establishing the optimal expression parameters for each construct. All purified

proteins were analyzed by SDS-PAGE and western blotting to verify purity and integrity before use in downstream assays.

GST pull-down assays

GST-OsRING20 and MBP-P10 fusion proteins were expressed in *E. coli* and purified as previously described. For each binding reaction, 10 μg of purified GST-OsRING20 or GST alone was incubated with GST beads at 4°C for 4 h with gentle rotation. Following incubation, 50 μL of protein supernatant containing MBP-P10 was added to each reaction and incubated for an additional 3 h at 4°C with gentle rotation. Beads were then pelleted by centrifugation (1,000 × g, 5 min, 4°C) and washed five times with ice-cold binding buffer. Bound proteins were eluted by boiling in 2× loading buffer containing 5% β-mercaptoethanol for 10 min at 100°C. Eluted proteins were resolved by 10% SDS-PAGE and analyzed by immunoblotting using Anti-GST antibody (clone 1B10, #ZB105A-1/ZB105A-2, Zomanbio, 1:5000) and Anti-MBP antibody (clone 7G2, #ZB108A-1/ZB108A-2, Zomanbio, 1:5000). In subsequent experiments, to validate additional protein-protein interactions, we employed a similar assay protocol, with only the expression vectors and corresponding target genes replaced.

RNA extraction and quantitative PCR analysis

Total RNA was isolated from rice leaf tissues using RNAiso Plus reagent (TaKaRa, Dalian, China) following the manufacturer's protocol. For cDNA synthesis, 1 μg of total RNA was first treated with DNase I (RNase-free) at 42°C for 2 min to eliminate genomic DNA contamination, followed by reverse transcription using 5×HiScript III qRT SuperMix (Vazyme Biotech, Nanjing, China) with random hexamer primers in a 20 μl reaction volume. The resulting cDNA was diluted to a working concentration of 100 ng/μl with nuclease-free water. Quantitative PCR was performed in triplicate technical replicates using AceQ qPCR SYBR Green Master Mix (Vazyme) on a QuantStudio 6 Flex Real-Time PCR System (Applied Biosystems) with the following cycling conditions: 95°C for 5 min; 40 cycles of 95°C for 10 sec and 60°C for 30 s; followed by a melt curve analysis. The rice *Actin 1* (*OsActin1*) gene served as the endogenous reference for normalization. For viral detection, the primer pairs targeting

554 the viral genes *P4*, *P8*, and *P10* are universally applicable for both RBSDV and
555 SRBSDV, as the two viruses share highly conserved sequences in these genomic
556 regions. Relative gene expression levels were calculated using the $2^{-\Delta\Delta Ct}$ method with
557 efficiency correction. Statistical analysis was performed using GraphPad Prism 9
558 software, with significance determined by Student's *t*-test for two-group comparisons
559 and One-way ANOVA with Tukey's post-hoc test for multiple comparisons. All
560 experiments included at least three independent biological replicates, with data
561 presented as mean ± standard deviation (SD).

562 **Protein extraction and western blotting analysis**

563 Total proteins were extracted from leaf tissues using an extraction buffer (100 mM
564 Tris-HCl, pH 6.8, 20% glycerol, 4% SDS, 0.2% bromphenol blue, 5%
565 β-mercaptoethanol). Protein samples were resolved by 10% sodium dodecyl
566 sulfate-polyacrylamide (SDS-PAGE) gels. Following electrophoresis, proteins were
567 transferred to NC membranes. Membranes were blocked with 5% non-fat dry milk in
568 TBST for 1 hour at room temperature or overnight. For immunodetection, membranes
569 were probed with specific monoclonal antibodies for 2 h at room temperature.
570 Antibodies against Flag (1:3000), GST (1:5000), GFP (1:5000) were used for protein
571 detection. After washing three times with TBST, membranes were incubated with
572 secondary antibodies at 37°C for 1 h. Goat anti-rabbit IgG (EASYBIO, BE0101) and
573 goat anti-mouse IgG horseradish peroxidase conjugate (Bio-Rad, 170-6516) were used
574 as secondary antibodies. Protein bands were visualized using enhanced
575 chemiluminescence substrate and imaged with a GE Chemiluminescence Imaging
576 System. Band intensities were quantified using ImageJ software with background
577 subtraction and normalization to loading controls.

578 ***In vitro* ubiquitination assays**

579 To determine OsRING20-mediated ubiquitination of P10, we performed in vitro
580 ubiquitination assays. The complete reaction mixture contained 50 ng wheat E1
581 (UBA1), 200-500 ng human E2 (UbcH5a), 5 μg Flag-ubiquitin, purified
582 His-OsRING20 and His-MBP-P10 proteins in ubiquitination buffer (25 mM Tris-HCl

pH 7.5, 50 mM NaCl, 5 mM ATP, 10 mM $MgCl_2$). Following incubation at 28°C for 2 h, reactions were terminated by addition of β-mercaptoethanol-supplemented loading buffer and boiling at 100°C for 5 min. Samples were resolved by 10-12% SDS-PAGE and analyzed by immunoblotting with anti-ubiquitin antibody (polyclonal, #30007ES50/30007ES60, Yeasen, 1:1000), anti-Flag antibody, and anti-His antibody (polyclonal, #0812-1, Huabio, 1:5000), and HRP-conjugated goat anti-Mouse IgG and HRP-conjugated goat anti-Rabbit IgG (#M21002, Abmart, 1:5000) were used as the secondary antibodies for immunodetection. In subsequent experiments, purified GST-P10 fusion protein was employed to conduct *in vitro* ubiquitination assays mediated by OsRING20 mutants, following the same protocol as described above.

***In vivo* ubiquitination assays**

To determine OsRING20-mediated ubiquitination of P10 in planta, we performed in vivo ubiquitination assays. Agrobacterium strains harboring P10-Flag and YFP-OsRING20 were co-infiltrated into *N. benthamiana* leaves. At 36 hours post-infiltration (hpi), leaf discs were treated with 100 μM MG132 or DMSO for an additional 12 h. Total proteins were extracted and immunoprecipitated with anti-Flag affinity beads. The ubiquitination level of P10-Flag was detected by immunoblotting with an anti-ubiquitin antibody (Yeasen, 1:1000). Experiments were repeated three times independently.

***In vivo* protein degradation assays**

To investigate P10 protein degradation in planta, we performed transient co-expression of YFP-OsRING20 and P10-Flag in *N. benthamiana* leaves. For proteasome inhibition assays, leaves were infiltrated with 100 μM MG132 (proteasome inhibitor), 100 μM E64d (autophagy inhibitor), or DMSO control at 16 hpi, with samples collected 16 h later (32 hpi total). Total proteins were analyzed by immunoblotting using anti-Flag and anti-GFP antibodies. To examine dose-dependent effects of OsRING20 on P10 degradation, we co-infiltrated Agrobacterium cultures containing P10-Flag (OD_{600}=0.5) with increasing concentrations of YFP-OsRING20 (OD_{600}=0, 0.25, 0.5, or 1.0), using YFP alone as negative control. Protein extracts from samples collected at 48 hpi were

similarly analyzed by western blotting to assess P10 stability relative to OsRING20 expression levels.

Cell-free protein degradation assays

Protein degradation assays were performed using a modified cell-free system. Total proteins were extracted from 0.5 g of rice leaves (ZH11 wild-type, OsRING20 knockout, and overexpression lines) in 1 mL of degradation buffer (25 mM Tris-HCl pH 7.5, 10 mM NaCl, 10 mM $MgCl_2$, 10 mM ATP, 5 mM DTT, 4 mM PMSF). To investigate proteasome-dependent degradation, the system was treated with 50 μM MG132 (proteasome inhibitor), E64d (autophagy inhibitor), MG132+E64d combination, DMSO vehicle control. Purified GST-P10 or GST (100 μg) were added to each reaction mixture, followed by incubation at 25°C. Aliquots were collected at 0, 1, and 2 h time points for immunoblot analysis using anti-GST antibody.

***In vitro* phase separation assays**

Prior to analysis, all recombinant proteins (YFP, YFP-OsRING20, and YFP-OsRING20-S45/46A) were clarified by centrifugation to remove potential aggregates. Protein concentrations were quantified using a NanoDrop spectrophotometer (A_{280} measurement). For phase separation assays, proteins were diluted in assay buffer (30 mM Tris-HCl pH 7.5, 150 mM NaCl, 1 mM DTT) to appropriate working concentrations and incubated at room temperature (25°C) for 30 min. Phase separation was subsequently assessed by fluorescence confocal microscopy (488 nm excitation), with images captured using consistent exposure settings across samples.

Fluorescence recovery after photobleaching (FRAP) analysis

FRAP experiments were conducted using a Nikon laser scanning confocal microscope. For *in planta* assays, *N. benthamiana* leaves were agroinfiltrated to express YFP-tagged OsRING20 (wild-type or mutant) and imaged at 2 dpi. Selected cytoplasmic granules were photobleached using three pulses of a 488 nm laser at 100% power, with subsequent recovery monitored by time-lapse imaging. For *in vitro* assays, purified protein droplets were subjected to a single bleach pulse at 50% laser power,

with ≥12 replicates analyzed per condition. All FRAP data were processed and recovery curves were generated using GraphPad Prism 9 software, following established analytical methods.

Confocal laser scanning microscopy and image processing

For live-cell imaging, *N. benthamiana* leaves agroinfiltrated with *Agrobacterium tumefaciens* (GV3101) containing various constructs were examined at 2 dpi using a Nikon A1R HD25 laser scanning confocal microscope. Fluorescence parameters were optimized as follows: GFP/YFP detection: 514 nm excitation, 530-600 nm emission; RFP detection: 633 nm excitation, 638-759 nm emission. All images were taken under a 20× objective lens combined with 15× optical/electronic zoom, yielding a total magnification of 300×.

Quantification of granules was conducted using image processing, following the established protocol with slight modifications (30). The YFP-OsRING20, YFP-OsRING20-S45/46A, YFP-OsRING20-dIDR1, YFP-OsRING20-dIDR2, and YFP-OsRING20-dRING were individually expressed in *N. benthamiana* leaves by agroinfiltration. Images were captured at 2 dpi under the same parameters (under a 20× objective lens combined with 5× optical/electronic zoom). Ten representative fields were imaged from at least five leaves. Raw images were processed in ImageJ by converting them to 8-bit grayscale and applying a threshold of 50-255. Granule numbers and sizes were quantified using the 'analyze particles' function (minimum size cutoff: 0.2 μm^2). For the statistical analysis of spontaneous condensate formation, a total of 500 randomly selected *N. benthamiana* epidermal cells expressing YFP-OsRING20 were examined. All data were exported to Excel for further analysis.

Generation of OsRING20-associated transgenic rice lines

To generate OsRING20 transgenic rice, both overexpression and knockout vectors were first constructed. The full-length OsRING20 coding sequence with an N-terminal Flag tag was cloned into the pCAMBIA1300 to create the pCAMBIA1300-Flag-OsRING20, while CRISPR guide RNAs were designed using CRISPR-P for knockout vector construction. Both constructs were independently

transformed into *Oryza sativa japonica* cv. Zhonghua 11 (ZH11) embryogenic calli via Agrobacterium-mediated transformation. Overexpression lines were verified through RT-qPCR analysis of transcript levels and confirmed by western blot using anti-Flag antibody. The knockout lines were screened by gDNA genotyping and confirmed by sequencing. For functional complementation, the relevant OsRING20 mutant variants were cloned into the pEarleyGate104 and independently transformed into *osring20* knockout background. Two overexpression lines with elevated expression and two homozygous mutant lines verified by genotyping were screened and used in this study.

Intrinsically disordered region (IDR) prediction

IDRs were predicted using PONDR® (Predictor of Natural Disordered Regions; http://www.pondr.com/) with default parameters.

Phylogenetic analysis

The full-length amino acid sequences of OsRING20 (XP_015639372.1) and its homologs from various plant species, including *Oryza brachyantha* (XP_040380633.1), *Arabidopsis thaliana* (NP_195130.1), *Nicotiana tabacum* (XP_016441339.1), *Brachypodium distachyon* (XP_010231670.1), *Triticum dicoccoides* (XP_037488037.1), *Triticum aestivum* (KAF6993995.1), and *Zea mays* (NP_001168137.1), were retrieved from NCBI (www.ncbi.nlm.nih.gov). For comparison, the amino acid sequences of established RING-H2 type E3 ligases from rice and Arabidopsis, namely OsBBI1 (Q9LWV9), OsHIP1 (Q7XTV7), AtMBR1 (Q9ZQF9), and AtCIP8 (Q9SPL2), were sourced from Uniprot (www.uniprot.org). All sequences were aligned using MEGA7 software. The phylogenetic tree was constructed using the neighbour-joining algorithm.

Quantification and statistical analysis

Protein band intensities from immunoblots were quantified using ImageJ software. For RT-qPCR data analysis, statistical significance was determined using Student's *t*-test for two-group comparisons or one-way analysis of variance (ANOVA) followed by Tukey's multiple comparison test for multi-group comparisons ($P < 0.05$; different letters above the bars indicate significant differences). All values are presented as mean

± SD. All statistical analyses were performed using GraphPad Prism 9 software.

References

1.F. Xu, H. Xue, The ubiquitin-proteasome system in plant responses to environments. *Plant Cell Environ*. **42**, 2931-2944 (2019).

2.G. Langin, M. González-Fuente, S. Üstün, The plant ubiquitin-proteasome system as a target for microbial manipulation. *Annu. Rev. Phytopathol*. **61**, 351–375 (2023).

3.Y. Hasegawa, Y. Luo, T. Sato, Recent advances in ubiquitin signals regulating plant membrane trafficking. *Plant Cell Physiol*. **65**, 1907-1924 (2024).

4.R.D. Vierstra, The ubiquitin-26S proteasome system at the nexus of plant biology. Nature reviews. *Nat. Rev. Mol. Cell Biol*. **10**, 385-397 (2009).

5.N. Zheng, N. Shabek, Ubiquitin ligases: structure, function, and regulation. *Annu. Rev. Biochem*. **86**, 129-157 (2017).

6.Z. Ban, M. Estelle, CUL3 E3 ligases in plant development and environmental response. *Nat. Plants* **7**, 6-16 (2021).

7.S. Toma-Fukai, T. Shimizu, Structural diversity of ubiquitin E3 ligase. *Molecules* **26**, 6682 (2021).

8.K.L. Lorick, J.P. Jensen, S. Fang, A.M. Ong, S. Hatakeyama, A.M. Weissman, RING fingers mediate ubiquitin-conjugating enzyme (E2)-dependent ubiquitination. *Proc. Natl. Acad. Sci. USA*. **96**, 11364-11369 (1999).

9.R.J. Deshaies, C.A. Joazeiro, RING domain E3 ubiquitin ligases. *Annu. Rev. Biochem*. **78**, 399-434 (2009).

10.L. Zeng, M.E. Vega-Sánchez, T. Zhu, G. Wang, Ubiquitination-mediated protein degradation and modification: an emerging theme in plant-microbe interactions. *Cell Res*. **16**, 413-426 (2006).

11.J. Verchot, Plant virus infection and the ubiquitin proteasome machinery: arms race along the endoplasmic reticulum. *Viruses* **8**, 314 (2016).

12.Z. Chen, J. Zhao, Q. Chen, Z. Zhang, J. Li, Z. Guo, Q. Xie, S. Ding, H. Guo, DNA geminivirus infection induces an imprinted E3 ligase gene to epigenetically activate viral gene transcription. *Plant Cell* **32**, 3256-3272 (2020).

13.L. Zhang, Y. Li, J.H. Kuhn, K. Zhang, Q. Song, F. Liu, Polyubiquitylated rice stripe virus NS3 translocates to the nucleus to promote cytosolic virus replication via miRNA-induced fibrillin 2 upregulation. *PLoS Pathog*. **20**, e1012112 (2024).

14.Y. Xie, M. Zeng, D. Wang, S. B. Gao, L. Li, L. Zheng, Y. Zhang, S. Fei, C. Zhang, Y. Wang, X. Zhou, J. Wu, Rice black-streaked dwarf virus-encoded P6 protein impairs OsPelota-mediated antiviral RNA decay defense via promoting OsSCE1b ubiquitination and degradation in rice. *J. Integr. Plant Biol.* **67**, 2760-2777 (2025).

15.J. Guo, T. Zhang, H. Xie, H. Hu, C. Shi, Y. Zhao, J. Yin, G. Xu, Z. Wu, P. Wang, J. Liu, P. Liu, K. Zhong, F. Chen, J. Chen, J. Yang, An m6A methyltransferase confers host resistance by degrading viral proteins through ubiquitination. *Nat. Commun.* **16**, 4821 (2025).

16.Z. Guo, X. Qin, H. Guo, C. Zheng, Z. Zhang, Q. Chen, X. Wang, C. Han, Y. Wang, The E3 ligase HRD1 enhances plant antiviral immunity by targeting viral movement proteins. *Cell Rep*. **44**, 115449 (2025).

17.Y. Huang, J. Yang, X. Sun, J. Li, X. Cao, S. Yao, Y. Han, C. Chen, L. Du, S. Li, Y. Ji, T. Zhou, H. Wang, J. J. Han, W. Wang, C. Wei, Q. Xie, Z. Yang, Y. Li, Perception of viral infections and initiation of antiviral defence in rice. *Nature* **641**, 173–181 (2025).
18.Y. He, G. Hong, H. Zhang, X. Tan, L. Li, Y. Kong, T. Sang, K. Xie, J. Wei, J. Li, F. Yan, P. Wang, H. Tong, C. Chu, J. Chen, Z. Sun, The OsGSK2 kinase integrates brassinosteroid and jasmonic acid signaling by interacting with OsJAZ4. *Plant Cell*. **32**, 2806-2822 (2020).
19.D. Lohse, X. Zhang, Physicochemical hydrodynamics of droplets out of equilibrium. *Nat. Rev. Phys*. **2**, 426-443 (2020).
20.R.J. Emenecker, A.S. Holehouse, L.C. Strader, Emerging roles for phase separation in plants. *Dev. Cell*. **55**, 69-83 (2020).
21.T. Wunder, O. Mueller-Cajar, Biomolecular condensates in photosynthesis and metabolism. *Curr. Opin. Plant Biol*. **58**, 1-7 (2020).
22.X. Liu, J. Zhu, C. Zhao, Liquid-liquid phase separation as a major mechanism of plant abiotic stress sensing and responses. *Stress Biol*. **3**, 56 (2023).
23.Q. Liu, W. Liu, Y. Niu, T. Wang, J. Dong, Liquid-liquid phase separation in plants: Advances and perspectives from model species to crops. *Plant Commun*. **5**, 100663 (2024).
24.K. Mäkinen, A. Lõhmus, M. Pollari, Plant RNA regulatory network and RNA granules in virus infection. *Front. Plant Sci*. **8**, 2093 (2017).
25.Y. Ding, R. Lozano-Durán, The cajal body in plant-virus interactions. *Viruses* **12**, 250 (2020).
26.G. Hoffmann, S. López-González, A. Mahboubi, J. Hanson, A. Hafrén, Cauliflower mosaic virus protein P6 is a multivalent node for RNA granule proteins and interferes with stress granule responses during plant infection. *Plant Cell* **35**, 3363-3382 (2023).
27.Q. Li, N. Liu, Q. Liu, X. Zheng, L. Lu, W. Gao, Y. Liu, Y. Liu, S. Zhang, Q. Wang, J. Pan, C. Chen, Y. Mi, M. Yang, X. Cheng, G. Ren, Y. Yuan, X. Zhang, DEAD-box helicases modulate dicing body formation in *Arabidopsis*. *Sci. Adv*. **7**, 6266 (2021).
28.S.L. Brown, D.J. Garrison, J.P. May, Phase separation of a plant virus movement protein and cellular factors support virus-host interactions. *PLoS Pathog*. **17**, e1009622 (2021).
29.S.L. Brown, J.P. May, Viral condensates formed by Pea enation mosaic virus 2 sequester ribosomal components and suppress translation. *Virology* **601**, 110301 (2025).
30.X. Fang, Q. Gao, Y. Zang, J. Qiao, D. Gao, W. Xu, Y. Wang, D. Li, X. Wang, Host casein kinase 1-mediated phosphorylation modulates phase separation of a rhabdovirus phosphoprotein and virus infection. *Elife* **11**, e74884 (2022).
31.X. Jing, P. Wang, J. Liu, M. Xiang, X. Song, C. Wang, P. Li, H. Li, Z. Wu, C. Zhang, A viral protein competitively bound to rice CIPK23 inhibits potassium absorption and facilitates virus systemic infection in rice. *Plant Biotechnol. J*. **22**, 2348-2363 (2024).
32.Z. Wang, J. Zhang, J. Huang, G. Sha, X. Song, X. Cao, Z. Yan, C. Liu, S. Chen, Z. Li, X. Huang, Q. Xie, X. Yang, G. Zhou, T. Zhang, Plant negative-strand RNA virus phosphoprotein condensates exploit host trafficking and lipid synthesis for viral factory assembly.*Sci. Adv.***11**, eadx7905 (2025).
33.M. Zeng, S. Fu, Y. Xu, L. Li, D. Wang, S. B. Gao, L. Zheng, Y. Zhang, C. Zhang, S. Fei, X. Ye., L. Chen, Y. Wang, T. Zhang, X. Zhou, J. Wu, Viral proteins suppress rice defenses by boosting OsTSN1 RNA decay via phase separation and multimerization. *Nat. Commun.* **16**, 7481 (2025).

34.H. M. Zhang, J. Chen, M. Adams, Molecular characterisation of segments 1 to 6 of Rice black-streaked dwarf virus from China provides the complete genome. *Arch. Virol.* **146**, 2331-2339 (2001).
35.S. A. Hogenhout, E. D. Ammar, A. E. Whitfield, M. G. Redinbaugh, Insect vector interactions with persistently transmitted viruses. *Annu. Rev. Phytopathol.* **46**, 327-359 (2008).
36.Y. Zhou, L. Zhang, X. Zhang, H. Zu, H. Di, L. Dong, X. Liu, X. Zeng, J. Weng, Z. Wang, Rice black-streaked dwarf virus genome in China: diversification, phylogeny, and selection. *Plant Dis.* **101**, 1588-1596 (2017).
37.P. Radivojac,V. Vacic, C. Haynes, R. R. Cocklin, A. Mohan, J. W. Heyen, M. G. Goebl, L. M. Iakoucheva. Identification, analysis, and prediction of protein ubiquitination sites. *Proteins*, **78,** 365-380 (2010).
38.L.M. Iakoucheva, P. Radivojac, C.J. Brown, T.R. O'Connor, J.G. Sikes, Z. Obradovic, A.K. Dunker, The importance of intrinsic disorder for protein phosphorylation. *Nucleic Acids Res.* **32**, 1037-1049 (2004).
39.H. Luo, Interplay between the virus and the ubiquitin-proteasome system: molecular mechanism of viral pathogenesis. *Curr. Opin. Virol*. **17**, 1-10 (2016).
40.E.H.G. Adams, S.H. Spoel, The ubiquitin-proteasome system as a transcriptional regulator of plant immunity. *J. Exp. Bot*. **69**, 4529–4537 (2018).
41.R. Mukherjee, I. Dikic, Regulation of host-pathogen interactions via the ubiquitin system. *Annu. Rev. Microbiol*. **76**, 211-233 (2022).
42.M.K. Isaacson, H.L. Ploegh, Ubiquitination, ubiquitin-like modifiers, and deubiquitination in viral infection. *Cell Host Microbe*. **5**, 559-570 (2009).
43.Q. Shen, T. Hu, M. Bao, L. Cao, H. Zhang, F. Song, Q. Xie, X. Zhou, Tobacco RING E3 ligase NtRFP1 mediates ubiquitination and proteasomal degradation of a Geminivirus-encoded βC1. *Mol. Plant* **9**, 911-25 (2016).
44.L. Liu, L. Jin, X. Huang, Y. Geng, F. Li, Q. Qin, R. Wang, S. Ji, S. Zhao, Q. Xie, C. Wei, C. Xie, B, Ding, Y. Li, OsRFPH2-10, a ring-H2 finger E3 ubiquitin ligase, is involved in rice antiviral defense in the early stages of rice dwarf virus infection. *Mol. Plant* **7**, 1057-1060 (2014).
45.B. Chen, L. Lin, Y. Lu, J. Peng, H. Zheng, Q. Yang, S. Rao, G. Wu, J. Li, Z. Chen, B. Song, J. Chen, F. Yan, Ubiquitin-Like protein 5 interacts with the silencing suppressor p3 of rice stripe virus and mediates its degradation through the 26S proteasome pathway. *PLoS Pathog*. **16**, e1008780 (2020).
46.L. Fan, Y. Zhou, X. Wei, W. Feng, H. Guo, Y. Li, X. Gao, J. Zhou, Y. Wen, Y. Wu, X. Shen, L. Liu, G. Xu, Z. Zhang, The E3 ligase TRIM22 restricts SARS-CoV-2 replication by promoting proteasomal degradation of NSP8. *mBio*. **15**, e0232023 (2024).
47.A.A. Hyman, C.A. Weber, F. Jülicher, Liquid-liquid phase separation in biology. *Annu. Rev. Cell Dev. Biol*. **30**, 39-58 (2014).
48.S. Alberti, A. Gladfelter, T. Mittag, Considerations and challenges in studying liquid-liquid phase separation and biomolecular condensates. *Cell* **176**, 419-434 (2019).
49.Y. Miao, X. Guo, K. Zhu, W. Zhao, Biomolecular condensates tunes immune signaling at the host-pathogen interface. *Curr. Opin. Plant Biol*. **74**, 102374 (2023).

50.L.D. Gallego, M. Schneider, C. Mittal, A. Romanauska, R.M. Gudino Carrillo, T. Schubert, B.F. Pugh, A. Köhler, Phase separation directs ubiquitination of gene-body nucleosomes. *Nature* **579**, 592-597 (2020).
51.R. Zavaliev, R. Mohan, T. Chen, X. Dong, Formation of NPR1 condensates promotes cell survival during the plant immune response. *Cell* **182**, 1093-1108.e18 (2020).
52.Z. Yang, G. Li, Y. Zhang, F. Li, T. Zhou, J. Ye, X. Wang, X. Zhang, Z. Sun, X. Tao, M. Wu, J. Wu, Y. Li, Crop antiviral defense: Past and future perspective. *Sci. China Life Sci*. **67**, 2617-2634 (2024).
53.W. Lin, P. D. Nagy, Co-opted cytosolic proteins form condensate substructures within membranous replication organelles of a positive-strand RNA virus. *New Phytol.* **243**, 1917-1935 (2024).
54.J. Zou, S. Zhang, Y. Chen, C. He, X. Pan, Y. Zhang, J. Xu, L. Zheng, H. Guan, M. Wu, D. Xie, Y. Ji, X. Fang, Y. Li, S. W. Ding, X. Fang, S. Zhao, J. Wu, A plant bunyaviral protein disrupts SERRATE phase separation to modulate microRNA biogenesis during viral pathogenesis. *Nat. Commun.* **16**, 6197 (2025).
55.A. M. Stanfield, J. P. May, Engineered Biomolecular Condensates Limit Tobacco Mosaic Virus Accumulation and Symptom Development. *Mol. Plant Pathol.* **26**, e70113 (2025).
56.P. Chakrabarti, D. Chakravarty, Intrinsically disordered proteins/regions and insight into their biomolecular interactions. *Biophys. Chem*. **283**, 106769 (2022).
57.E.W. Martin, A.S. Holehouse, Intrinsically disordered protein regions and phase separation: sequence determinants of assembly or lack thereof. *Emerg. Top. Life Sci*. **4**, 307-329 (2020).
58.I. Owen, F. Shewmaker, The role of post-translational modifications in the phase transitions of intrinsically disordered proteins. *Int. J. Mol. Sci*. **20**, 5501 (2019).
59.H. Bae, J.H. Sohn, The ubiquitin-proteasome system in rice: genome-wide analysis and functional interpretation.*Plant Cell* **114**, 179-189 (2013).
60.R. Wang, X. Xu, G. Wang, Y. Ning, Ubiquitination of susceptibility proteins modulates rice broad-spectrum resistance. *Trends Plant Sci*. **27**, 322-324 (2022).
61.Y. Yan, H. Wang, Y. Bi, F. Song, Rice E3 ubiquitin ligases: From key modulators of host immunity to potential breeding applications. *Plant Commun*. **5**, 101128 (2024).
62.C. Zhang, H. Fang, J. Wang, H. Tao, D. Wang, M. Qin, F. He, R. Wang, G. Wang, Y. Ning, The rice E3 ubiquitin ligase-transcription factor module targets two trypsin inhibitors to enhance broad-spectrum disease resistance. *Dev Cell* **59**, 2270-2271 (2024).
63.S. Fu, K. Wang, T. Ma, Y. Liang, Z. Ma, J. Wu, Y. Xu, X. Zhou, An evolutionarily conserved C4HC3-type E3 ligase regulates plant broad-spectrum resistance against pathogens. *Plant Cell* **34**, 1822-1843 (2022).
64.Y. Bi, H. Wang, X. Yuan, Y. Yan, D. Li, F. Song, The NAC transcription factor ONAC083 negatively regulates rice immunity against *Magnaporthe oryzae* by directly activating transcription of the RING-H2 gene OsRFPH2-6. *J. Integr. Plant Biol*. **65**, 854-875 (2023).
65.S. Wang, S. Han, X. Zhou, C. Zhao, L. Guo, J. Zhang, F. Liu, Q. Huo, W. Zhao, Z. Guo, X. Chen, Phosphorylation and ubiquitination of OsWRKY31 are integral to OsMKK10-2-mediated defense responses in rice. *Plant Cell* **35**, 2391-2412 (2023).
66.Y. Yan, H. Wang, Y. Bi, J. Wang, D. Li, F. Song, A distinct protein posttranslational modifications-linked OsATL32-OsPPKL2-OsGSK2 loop modulates rice immunity against blast disease. *New Phytol*. **243**, 2332-2350 (2024).

67.Y. Yan, H. Wang, Y. Bi, J. Wang, M. Noman, D. Li, F. Song, OsATL32 ubiquitinates the reactive oxygen species-producing OsRac5-OsRbohB module to suppress rice immunity. *J. Integr. Plant Biol*. **66**, 1459-1480 (2024).
68.S. Tatineni, G.L. Hein, Plant viruses of agricultural importance: Current and future perspectives of virus disease management strategies. *Phytopathology* **113**, 117-141 (2023).
69.M. Gao, E. Aguilar, B. Garnelo Gómez, L. Medina-Puche, P. Fan, I. Ontiveros, S. Pan, H. Tan, H. Wei, E. von Roepenack-Lahaye, N. Chen, X.-W. Wang, D. C. Baulcombe, E. R. Bejarano, J. A. Díaz-Pendón, M. Furutani, M. T. Morita, R. Lozano-Durán, A plant virus causes symptoms through the deployment of a host-mimicking protein domain to attract the insect vector. *Mol. Plant.* **18,** 1029-1046 (2025).
70.Y. Mei, Y. Wang, F. Li, R. Lozano-Durán, X. Zhou, Defence-mediated phloem restriction of a plant virus facilitates insect transmission. *Nat. Commun* **17**, 152 (2025).
71.A. Hanzl, G.E. Winter, Targeted protein degradation: current and future challenges. *Curr. Opin. Chem. Biol*. **56**, 35-41 (2020).
72.P. Zhao, H. Yang, Y. Sun, J. Zhang, K. Gao, J. Wu, C. Zhu, C. Yin, X. Chen, Q. Liu, Q. Xia, Q. Li, H. Xiao, H. Sun, X. Zhang, L. Yi, C. Zhou, D.J. Kliebenstein, R. Fang, X. Wang, J. Ye, Targeted MYC2 stabilization confers citrus Huanglongbing resistance. *Science* **388**, 191-198 (2025).
73.C. Opachaloemphan, S. He, A natural defense against plant disease. *Science* **388**, 149-150 (2025).

Acknowledgements

We are grateful to Prof. Yuese Ning (State Key Laboratory for Biology of Plant Diseases and Insect Pests, Institute of Plant Protection, Chinese Academy of Agricultural Sciences) for his expert guidance on ubiquitination assays, and to Prof. Tao Li (College of Life Science, Henan Agricultural University) for his valuable advice on FRAP experimental design and analysis.

Funding:

The project is supported by National Natural Science Foundation of China grant 32572784 (C. Zhang), High-level Talents-Top Talents Project of Henan Agricultural University grant 30500948 (C. Zhang), and School-Enterprise Cooperation Project grant 30803130 (C. Zhang).

Author contributions:

Conceptualization: P.L. and C.Z.; Methodology: M.X., P.W., X.J., H. X., Z.Z., B.Q., P.Z., F.D., Z,l., and C.W.; Investigation: M.X., P.L., P.W., X.J.,and C.Z.;

Visualization: M.X., and P.W.; Supervision: P.L., H.L., Z.W., and C.Z.; Writing-original draft: M.X., P.L., and C.Z.; Writing-review & editing: P.L., M.X., P.W., and C.Z.

Conflict of interest

The authors declare that there is no conflict of interest.

Data availability statement

The data supporting the findings of this study are available within the paper and its Supplementary Information.

Main Figure Legends

Fig. 1. OsRING20 interacts directly with RBSDV P10 *in vitro* and *in vivo*. (A) Predicted structural model of the OsRING20-P10 binding interface. **(B)** Yeast two-hybrid (Y2H) assay confirmed the direct interaction between OsRING20 and P10 under stringent conditions (SD/–Trp/–Leu/–His/–Ade and SD/–Trp/–Leu/–His/–Ade+X-α-gal). **(C)** Bimolecular fluorescence complementation (BiFC) assay for the OsRING20-P10 interaction in *N. benthamiana* leaves. YFP signals (green) from OsRING20-nYFP/P10-cYFP and P10-nYFP/OsRING20-cYFP localize to nuclear puncta. The nucleus was labeled with H2B-RFP. Bright field (BF). Scale bars, 5 μm.

(D) Co-IP assay for the OsRING20-P10 interaction. P10-Flag was co-expressed with YFP-OsRING20 or a YFP control in *Nicotiana benthamiana* leaves. Immunoprecipitation with anti-GFP and immunoblot analysis with anti-Flag. **(E)** *In vitro* pull-down assay demonstrating specific binding between P10 and OsRING20. Purified GST or GST-OsRING20 was used to pull down MBP-fused P10, and the pull-down fractions were analyzed by immunoblotting with anti-MBP antibody, the input samples were further immunoblotted using anti-GST antibody.

Fig. 2. OsRING20 functions as an E3 ubiquitin ligase to ubiquitinate P10 and target it for proteasome-dependent degradation. (A) *In vitro* ubiquitination assay determining the polyubiquitination of P10 catalyzed by OsRING20. Reaction mixtures containing purified MBP-P10 were incubated with E1, E2, ubiquitin, and Flag-tagged OsRING20. The P10 ubiquitination was detected by immunoblotting with both anti-His and anti-Ub antibodies. **(B)** *In planta* degradation assays showing the proteasome-dependent degradation of P10 mediated by OsRING20. Flag-tagged P10 was co-expressed with YFP-OsRING20 or YFP control in *Nicotiana benthamiana* leaves. The accumulation levels of P10 were analyzed by immunoblotting with anti-Flag antibody. An anti-Actin antibody was used to detect NbActin as a loading control. **(C)** Cell-free degradation assay showing P10 degradation in protein extracts from ZH11, *OsRING20*-overexpression, and *OsRING20*-knockout plants. Purified GST-P10 was incubated with total protein extracts from the indicating rice seedlings. P10 degradation was monitored hourly by immunoblotting with anti-GST antibody. 100 μM MG132 was added to inhibiting proteasome activity. These experiments were performed with three independent biological replicates with similar results.

Fig. 3. The RING domain is indispensable for OsRING20 self-interaction, E3 ligase activity, and P10 degradation. (A) Predicted structural model of the OsRING20 homodimer, highlighting the interaction interface. **(B)** Domain architecture of wild-type OsRING20 and the RING domain deletion mutant (dRING). **(C)** Yeast two-hybrid (Y2H) assay showing OsRING20-dRING self-interaction and interaction with P10 under stringent selection (SD/-Trp/-Leu/-His/-Ade). **(D)**

Bimolecular fluorescence complementation (BiFC) assay confirming OsRING20-dRING self-interaction and interaction with P10. YFP signals (green) from OsRING20-nYFP/OsRING20-cYFP, OsRING20-dRING-nYFP/P10-cYFP, and P10-nYFP/OsRING20-dRING-cYFP localize to nuclear puncta. The nucleus was labeled with H2B-RFP. Bright field (BF). Scale bars, 5 μm. **(E)** *In vitro* ubiquitination assay demonstrating that OsRING20-dRING fails to catalyze P10 polyubiquitination. The P10 ubiquitination was detected by immunoblotting with both anti-GST and anti-Ub antibodies. **(F)** *In planta* degradation assay. Flag-tagged P10 was co-expressed with YFP-OsRING20, YFP-OsRING20-dRING, or YFP control in *Nicotiana benthamiana* leaves. The accumulation levels of P10 were analyzed by immunoblotting with anti-Flag antibody. An anti-Actin antibody was used to detect NbActin as a loading control.

Fig. 4. Identification and functional validation of ubiquitination sites in P10. (A) UbPred bioinformatic analysis predicted five potential ubiquitination sites in P10, with K363 and K555 identified as high-confidence sites. **(B)** Yeast two-hybrid (Y2H) assay confirmed the direct interaction between OsRING20 and P10-K363/555A under stringent conditions (SD/–Trp/–Leu/–His/–Ade and SD/–Trp/–Leu/–His/–Ade+X-α-gal). **(C)** Bimolecular fluorescence complementation (BiFC) assay for the OsRING20-P10-K363/555A interaction in *Nicotiana benthamiana* leaves. YFP signals (green) from OsRING20-nYFP/P10-K363/555A-cYFP and P10-K363/555A-nYFP/OsRING20-cYFP still localize to nuclear puncta. The nucleus was labeled with H2B-RFP. Bright field (BF). Scale bars, 5 μm. **(D)** Co-IP assay for the OsRING20-P10-K363/555A interaction. P10-K363/555A-Flag was co-expressed with YFP-OsRING20 or a YFP control in *N. benthamiana* leaves. Immunoprecipitation with anti-GFP and immunoblot analysis with anti-Flag. **(E)** *In vitro* pull-down assay demonstrating specific binding between P10-K363/555A and OsRING20. Purified GST or GST-OsRING20 was used to pull down MBP-fused P10-K363/555A, and the pull-down fractions were analyzed by immunoblotting with anti-MBP antibody. **(F)** *In vitro* ubiquitination assay determining

the polyubiquitination of P10-K363/555A catalyzed by His-YFP-OsRING20. Reaction mixtures containing purified MBP-P10-K363/555A were incubated with E1, E2, ubiquitin, and Flag-tagged His-YFP-OsRING20. The P10-K363/555A ubiquitination was detected by immunoblotting with both anti-His and anti-Ub antibodies. **(G)** *In planta* degradation assay demonstrating that the P10-K363/555A mutant resists OsRING20-mediated degradation. Flag-tagged P10-K363/555A was co-expressed with YFP-OsRING20 or YFP control in *N. benthamiana* leaves. The accumulation levels of P10-K363/555A were analyzed by immunoblotting with anti-Flag antibody. An anti-Actin antibody was used to detect NbActin as a loading control.

Fig. 5. OsRING20 undergoes liquid-liquid phase separation (LLPS) *in vivo* and *in vitro*. (A) Confocal microscopy images showing nuclear localization of OsRING20 in plant cells. Bright field (BF). Scale bars, 5 μm. **(B)** Quantitative analysis of spontaneous formation of spherical liquid-like condensates by OsRING20. A total of 500 randomly selected *N. benthamiana* epidermal cells expressing YFP-OsRING20 were counted. **(C)** Prediction of intrinsically disordered regions (IDR1 and IDR2) in OsRING20 by PONDR analysis. **(D)** FRAP of YFP-OsRING20 expressed in epidermal cells of *N. benthamiana* leaves. The red circles indicate the non-photobleached nuclear condensate. The white circles indicate the photobleached nuclear condensate. Scale bars, 5 μm. **(E)** Relative fluorescence recovery curves of photobleached YFP-OsRING20. Data were normalized by the web-based tool easy FRAP. Red lines for unbleached; green lines for bleached. **(F)** FRAP of the interior region of a YFP-OsRING20 condensate in *N. benthamiana* leaf epidermal cells. White circles indicate the photobleached area. **(G)** Relative fluorescence recovery curves of YFP-OsRING20 photobleached within the interior region of a condensate. green lines for bleached. **(H, I)** Expression and purification of His-YFP-OsRING20 fusion protein. (H) Fluorescence imaging of purified His-YFP and His-YFP-OsRING20 proteins. (I) Western blot analysis of purified His-YFP and His-YFP-OsRING20 proteins using an anti-GFP antibody. **(J)** *In vitro* reconstitution

of liquid condensates by His-YFP-OsRING20 under 500 mM NaCl treatment. Bright field (BF). Scale bars, 5 μm. **(K)** FRAP analysis of YFP-OsRING20 in vitro condensates. The photobleached area is circled in white. Scale bars, 5 μm. **(L)** Relative fluorescence recovery curve of YFP-OsRING20 after photobleaching in the in vitro condensate. green lines for bleached. **(M)** Time-lapse images showing fission of OsRING20 condensates and fusion *in vivo*. Scale bars, 5 μm.

Fig. 6. IDR1 and Ser45/46 are critical to the liquid-liquid phase separation (LLPS) of OsRING20 and facilitates of P10 protein degradation. (A) Domain architecture of OsRING20 and its truncation mutants. **(B)** Confocal microscopy images showing condensate formation of wild-type OsRING20, OsRING20-dIDR1, OsRING20-dIDR2, and OsRING20-dRING in plant nuclei. The nucleus was labeled with H2B-RFP. Bright field (BF). Scale bars, 5 μm. **(C, D)** FRAP (C) and recovery curves (D) of wild-type OsRING20 and its mutants. Scale bars, 5 μm. **(E)** Confocal microscopy images showing condensate formation of wild-type OsRING20 and OsRING20-S45/46A in plant nuclei. Bright field (BF). Scale bars, 5 μm. **(F, G)** FRAP analysis demonstrating impaired dynamics of OsRING20-S45/46A mutant. FRAP (F) and recovery curves (G). Scale bars, 5 μm. **(H, I)** *In planta* degradation assays demonstrating impaired P10 degradation by phase separation-deficient mutants. Flag-tagged P10 was co-expressed with YFP-OsRING20, YFP-OsRING20-dIDR1, YFP-OsRING20-S45/46A, or YFP control in *Nicotiana benthamiana* leaves. The accumulation levels of P10 were analyzed by immunoblotting with anti-Flag antibody. The accumulation levels of YFP-OsRING20, YFP-OsRING20-dIDR1(H), YFP-OsRING20-S45/46A(I), or YFP control were analyzed by immunoblotting with anti-GFP antibody. An anti-Actin antibody was used to detect NbActin as a loading control.

Fig. 7. The viral P10 promotes liquid-liquid phase separation (LLPS) of OsRING20. (A) Representative confocal microscopy images of *Nicotiana benthamiana* epidermal cells co-expressing YFP-OsRING20 with either P10-Flag or a GUS-Flag control. Scale bars, 5 μm. **(B)** Quantification of cells containing OsRING20

condensates in the presence of P10 or GUS. **(C)** Immunoblot analysis confirming comparable expression levels of YFP-OsRING20 in samples from (A), using anti-GFP antibody. An anti-Flag antibody was used to detect the presence of P10. **(D)** *In vitro* condensate formation assay showing the phase separation of His-YFP-OsRING20 incubated with purified GST-P10 or GST control under 800 mM NaCl. Scale bars, 50 μm. **(E)** Quantification of cells containing OsRING20 condensates in the presence of GST-P10 or GST under 800 mM NaCl. **(F)** Western blot showing comparable expression levels of YFP-OsRING20 across experimental groups (E). **(G)** Coomassie brilliant blue stained SDS-PAGE gel of purified GST-P10, GST, and His-YFP-OsRING20. **(H)** Western blot analysis of native PAGE gel showing His-YFP-OsRING20 under increasing NaCl concentrations (0, 500, and 1000 mM). **(I)** Western blot of native PAGE gel subjected with His-YFP-OsRING20 incubated with GST-P10 or GST alone. Red asterisks indicate the targeted proteins.

Fig. 8. OsRING20 confers RBSDV resistance without causing obvious vegetative growth defects in rice. (A) Morphology of wild-type (ZH11), empty vector (E.V.), *OsRING20*-overexpression (OE) and *OsRING20*-knockout (KO) plants under normal growth conditions. Scale bars, 15 cm. **(B)** Sequencing chromatograms verifying targeted mutations in two independent *OsRING20* KO lines. **(C, D)** Validation of *OsRING20* overexpression in two OE lines through RT-qPCR (C) and Western blot (D) analysis. **(E)** Disease resistance evaluation of *OsRING20*. Disease symptoms in the indicated genotypes following RBSDV infection. Scale bars, 15 cm. **(F)** RT-qPCR analysis of RBSDV *P4*, *P8*, and *P10* transcript levels in plants from (E). **(G)** Disease resistance evaluation of transgenic complemented lines with wild-type OsRING20 or its mutants in the *OsRING20* KO background following RBSDV infection. Scale bars, 5 cm. **(H)** RT-qPCR analysis of RBSDV *P4*, *P8*, and *P10* transcript levels in plants from (G). Statistical analysis was performed via one-way analysis of variance (ANOVA) with Tukey's multiple comparison test. Different letters above the bars indicate significant differences among the treatments at the $P<0.05$ level. These

experiments were performed with three independent biological replicates with similar results.

Fig. 9. OsRING20 enhances antiviral resistance by targeting SRBSDV capsid proteins for degradation. (A) Structural model predicting OsRING20-SP10 binding interface. **(B)** Bimolecular fluorescence complementation (BiFC) assay confirming the interaction between OsRING20 and SP10 in *Nicotiana benthamiana* leaves. YFP signals (green) from OsRING20-nYFP/SP10-cYFP and SP10-nYFP/OsRING20-cYFP localize to nuclear puncta. The nucleus was labeled with H2B-RFP. Bright field (BF). Scale bars, 5 μm. **(C)** *In vitro* GST pull-down assay demonstrating direct binding between OsRING20 and SP10. The GST-fused OsRING20-pull-down fractions were analyzed by immunoblotting with anti-MBP antibody. **(D)** *In planta* degradation assay showing OsRING20-mediated SP10 degradation. Flag-tagged SP10 was co-expressed with YFP-OsRING20, YFP-OsRING20-dRING, or YFP control in *N. benthamiana* leaves, respectively. The accumulation levels of SP10 were analyzed by immunoblotting with anti-Flag antibody. An anti-Actin antibody was used to detect NbActin as a loading control. **(E)** Cell-free degradation assay validating SP10 degradation by OsRING20. Purified MBP-SP10 was incubated with total protein extracts from ZH11, *OsRING20*-overexpression, and *OsRING20*-knockout rice seedlings. P10 degradation was monitored hourly by immunoblotting with anti-MBP antibody. **(F)** Disease resistance evaluation of complementation lines with wild-type *OsRING20* and its mutants in the *OsRING20* KO background following SRBSDV infection. Scale bars, 5 cm. **(G, H)** RT-qPCR analysis of SRBSDV *SP8* (G) and *SP10* (H) transcript levels in plants from (F). Statistical analysis was performed via one-way analysis of variance (ANOVA) with Tukey's multiple comparison test. Different letters above the bars indicate significant differences among the treatments at the $P<0.05$ level. These experiments were performed with three independent biological replicates with similar results. **(I)** Immunoblot analysis of SP10 protein accumulation in plants from (F). Rice Actin serves as the loading control.

Fig. 10. A working model indicating that the phase-separated OsRING20 drives antiviral resistance through targeting viral capsid proteins for UPS-dependent degradation. Upon virus infection and the subsequent recognition of viral CPs trigger OsRING20 phase separation. The resulting biomolecular condensates are essential for the OsRING20-mediated ubiquitination and degradation of viral CPs, thereby establishing its antiviral function.

Fig. 1

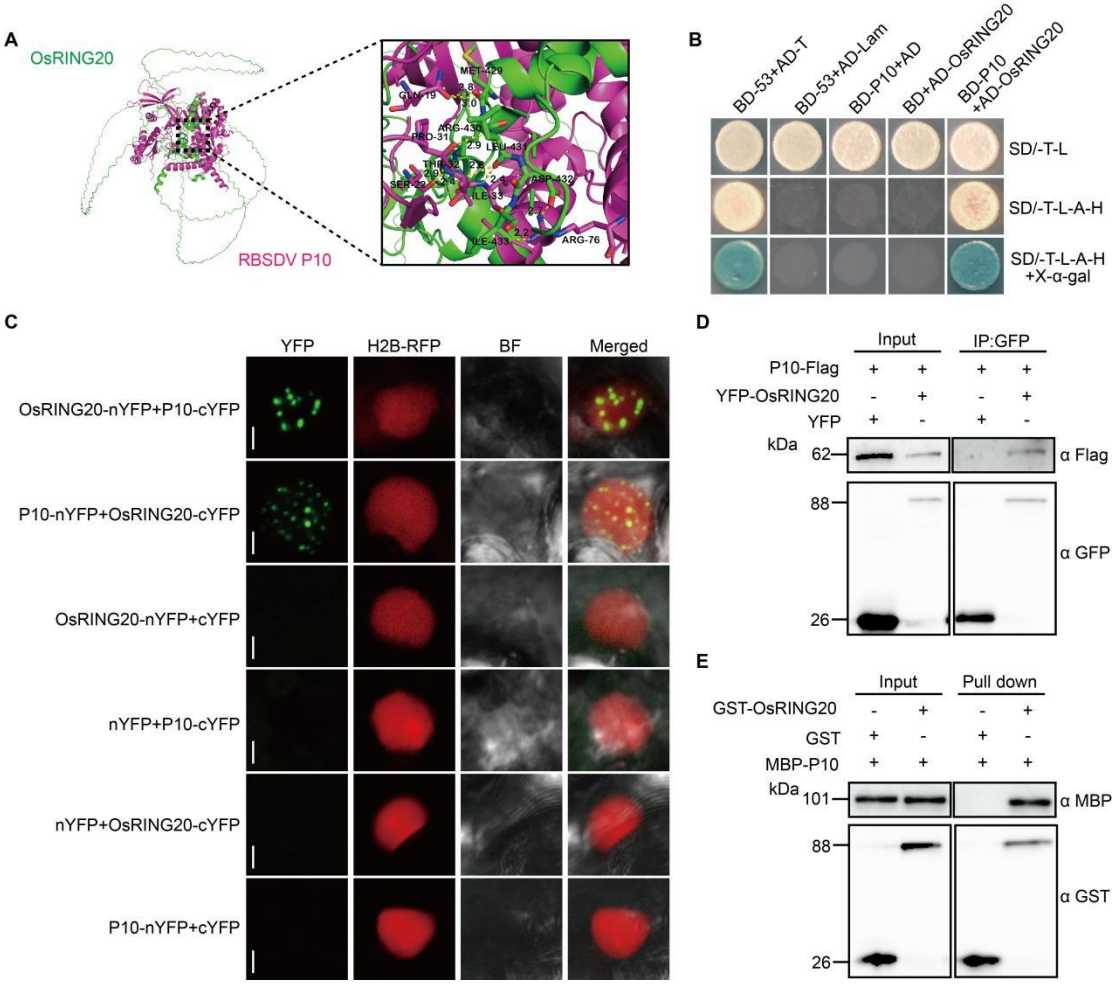

A
OsRING20
RBSDV P10
B
BD-53+AD-T
BD-53+AD-Lam
BD-P10+AD
BD+AD-OsRING20
BD-P10 +AD-OsRING20
SD/-T-L
SD/-T-L-A-H
SD/-T-L-A-H +X-α-gal
C
YFP
H2B-RFP
BF
Merged
OsRING20-nYFP+P10-cYFP
P10-nYFP+OsRING20-cYFP
OsRING20-nYFP+cYFP
nYFP+P10-cYFP
nYFP+OsRING20-cYFP
P10-nYFP+cYFP
D
Input
IP:GFP
P10-Flag
YFP-OsRING20
YFP
kDa
62
88
26
α Flag
α GFP
E
Input
Pull down
GST-OsRING20
GST
MBP-P10
kDa
101
88
26
α MBP
α GST

Fig. 2

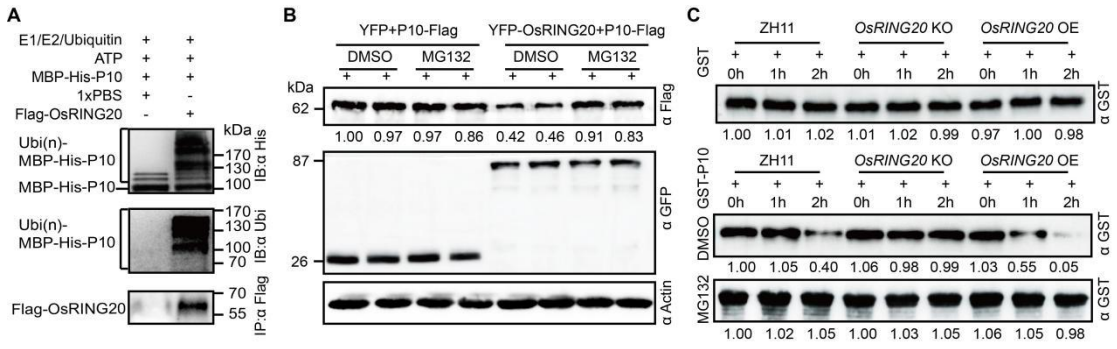

A
E1/E2/Ubiquitin + +
ATP + +
MBP-His-P10 + +
1xPBS + -
Flag-OsRING20 - +
kDa
Ubi(n)-MBP-His-P10
MBP-His-P10
170
130
100
IB:α His
Ubi(n)-MBP-His-P10
170
130
100
70
IB:α Ubi
Flag-OsRING20
70
55
IP:α Flag
B
YFP+P10-Flag
YFP-OsRING20+P10-Flag
DMSO
MG132
DMSO
MG132
kDa
62
1.00 0.97 0.97 0.86 0.42 0.46 0.91 0.83
α Flag
87
26
α GFP
α Actin
C
ZH11
OsRING20 KO
OsRING20 OE
GST
0h 1h 2h 0h 1h 2h 0h 1h 2h
1.00 1.01 1.02 1.01 1.02 0.99 0.97 1.00 0.98
α GST
GST-P10
DMSO
1.00 1.05 0.40 1.06 0.98 0.99 1.03 0.55 0.05
MG132
1.00 1.02 1.05 1.00 1.03 1.05 1.06 1.05 0.98

Fig. 3

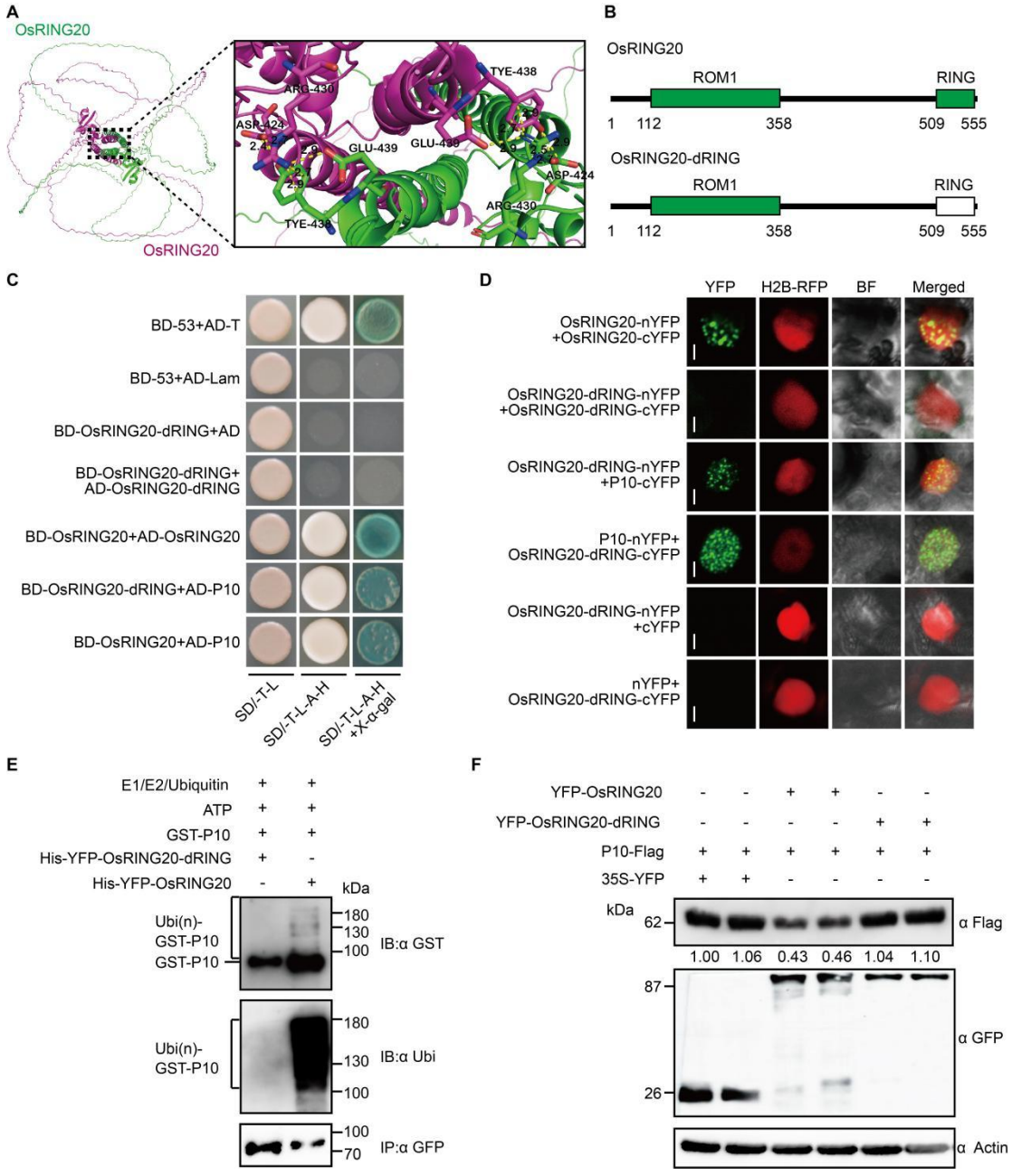

A
OsRING20
TYE-438
ARG-430
ASP-424
GLU-439
GLU-439
ASP-424
ARG-430
TYE-438
OsRING20
B
OsRING20
ROM1
RING
1
112
358
509
555
OsRING20-dRING
ROM1
RING
1
112
358
509
555
C
BD-53+AD-T
BD-53+AD-Lam
BD-OsRING20-dRING+AD
BD-OsRING20-dRING+
AD-OsRING20-dRING
BD-OsRING20+AD-OsRING20
BD-OsRING20-dRING+AD-P10
BD-OsRING20+AD-P10
SD/-T-L
SD/-T-L-A-H
SD/-T-L-A-H
+X-α-gal
D
YFP
H2B-RFP
BF
Merged
OsRING20-nYFP
+OsRING20-cYFP
OsRING20-dRING-nYFP
+OsRING20-dRING-cYFP
OsRING20-dRING-nYFP
+P10-cYFP
P10-nYFP+
OsRING20-dRING-cYFP
OsRING20-dRING-nYFP
+cYFP
nYFP+
OsRING20-dRING-cYFP
E
E1/E2/Ubiquitin + +
ATP + +
GST-P10 + +
His-YFP-OsRING20-dRING + -
His-YFP-OsRING20 - +
kDa
Ubi(n)-
GST-P10
GST-P10
180
130
100
IB:α GST
Ubi(n)-
GST-P10
180
130
100
IB:α Ubi
100
70
IP:α GFP
F
YFP-OsRING20 - - + + - -
YFP-OsRING20-dRING - - - - + +
P10-Flag + + + + + +
35S-YFP + + - - - -
kDa
62
α Flag
1.00 1.06 0.43 0.46 1.04 1.10
87
26
α GFP
α Actin

Fig. 4

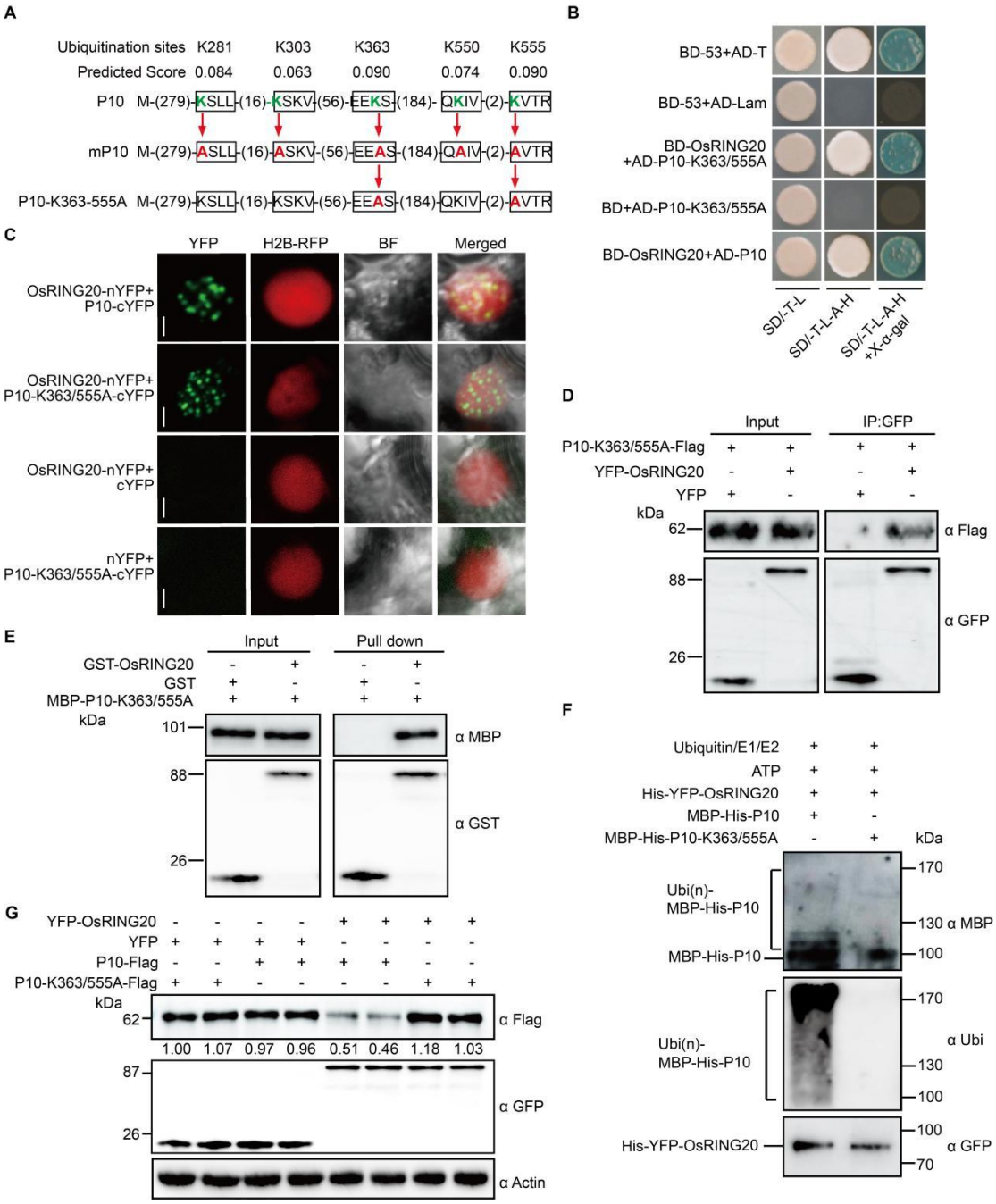

A
Ubiquitination sites K281 K303 K363 K550 K555
Predicted Score 0.084 0.063 0.090 0.074 0.090
P10 M-(279)-KSLL-(16)-KSKV-(56)-EEKS-(184)-QKIV-(2)-KVTR
mP10 M-(279)-ASLL-(16)-ASKV-(56)-EEAS-(184)-QAIV-(2)-AVTR
P10-K363-555A M-(279)-KSLL-(16)-KSKV-(56)-EEAS-(184)-QKIV-(2)-AVTR
B
BD-53+AD-T
BD-53+AD-Lam
BD-OsRING20 +AD-P10-K363/555A
BD+AD-P10-K363/555A
BD-OsRING20+AD-P10
SD/-T-L
SD/-T-L-A-H
SD/-T-L-A-H +X-α-gal
C
YFP
H2B-RFP
BF
Merged
OsRING20-nYFP+ P10-cYFP
OsRING20-nYFP+ P10-K363/555A-cYFP
OsRING20-nYFP+ cYFP
nYFP+ P10-K363/555A-cYFP
D
Input
IP:GFP
P10-K363/555A-Flag + + + +
YFP-OsRING20 - + - +
YFP + - + -
kDa
62
88
26
α Flag
α GFP
E
Input
Pull down
GST-OsRING20 - + - +
GST + - + -
MBP-P10-K363/555A + + + +
kDa
101
88
26
α MBP
α GST
F
Ubiquitin/E1/E2 + +
ATP + +
His-YFP-OsRING20 + +
MBP-His-P10 + -
MBP-His-P10-K363/555A - +
kDa
Ubi(n)-MBP-His-P10
MBP-His-P10
170
130
100
α MBP
Ubi(n)-MBP-His-P10
170
130
100
α Ubi
His-YFP-OsRING20
100
70
α GFP
G
YFP-OsRING20 - - - - + + + +
YFP + + + + - - - -
P10-Flag - - + + + + - -
P10-K363/555A-Flag + + - - - - + +
kDa
62
1.00 1.07 0.97 0.96 0.51 0.46 1.18 1.03
α Flag
87
26
α GFP
α Actin

Fig. 5

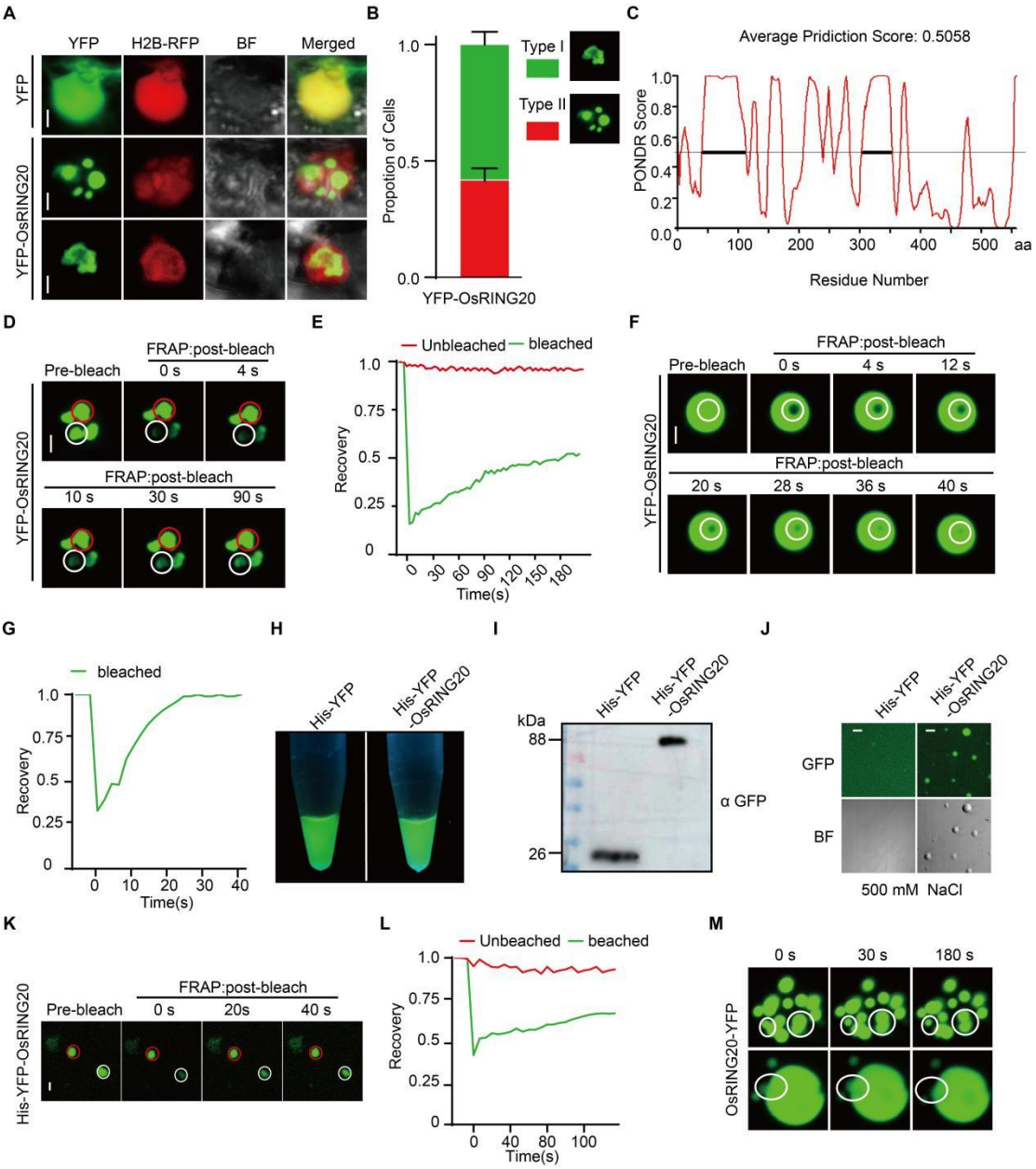

A
YFP
H2B-RFP
BF
Merged
YFP
YFP-OsRING20
B
Propotion of Cells
Type I
Type II
YFP-OsRING20
C
Average Pridiction Score: 0.5058
PONDR Score
Residue Number
aa
D
FRAP:post-bleach
Pre-bleach
0 s
4 s
10 s
30 s
90 s
YFP-OsRING20
E
Unbleached
bleached
Recovery
Time(s)
F
FRAP:post-bleach
Pre-bleach
0 s
4 s
12 s
20 s
28 s
36 s
40 s
YFP-OsRING20
G
bleached
Recovery
Time(s)
H
His-YFP
His-YFP -OsRING20
I
kDa
88
26
His-YFP
His-YFP -OsRING20
α GFP
J
His-YFP
His-YFP -OsRING20
GFP
BF
500 mM NaCl
K
His-YFP-OsRING20
FRAP:post-bleach
Pre-bleach
0 s
20s
40 s
L
Unbeached
beached
Recovery
Time(s)
M
0 s
30 s
180 s
OsRING20-YFP

Fig. 6

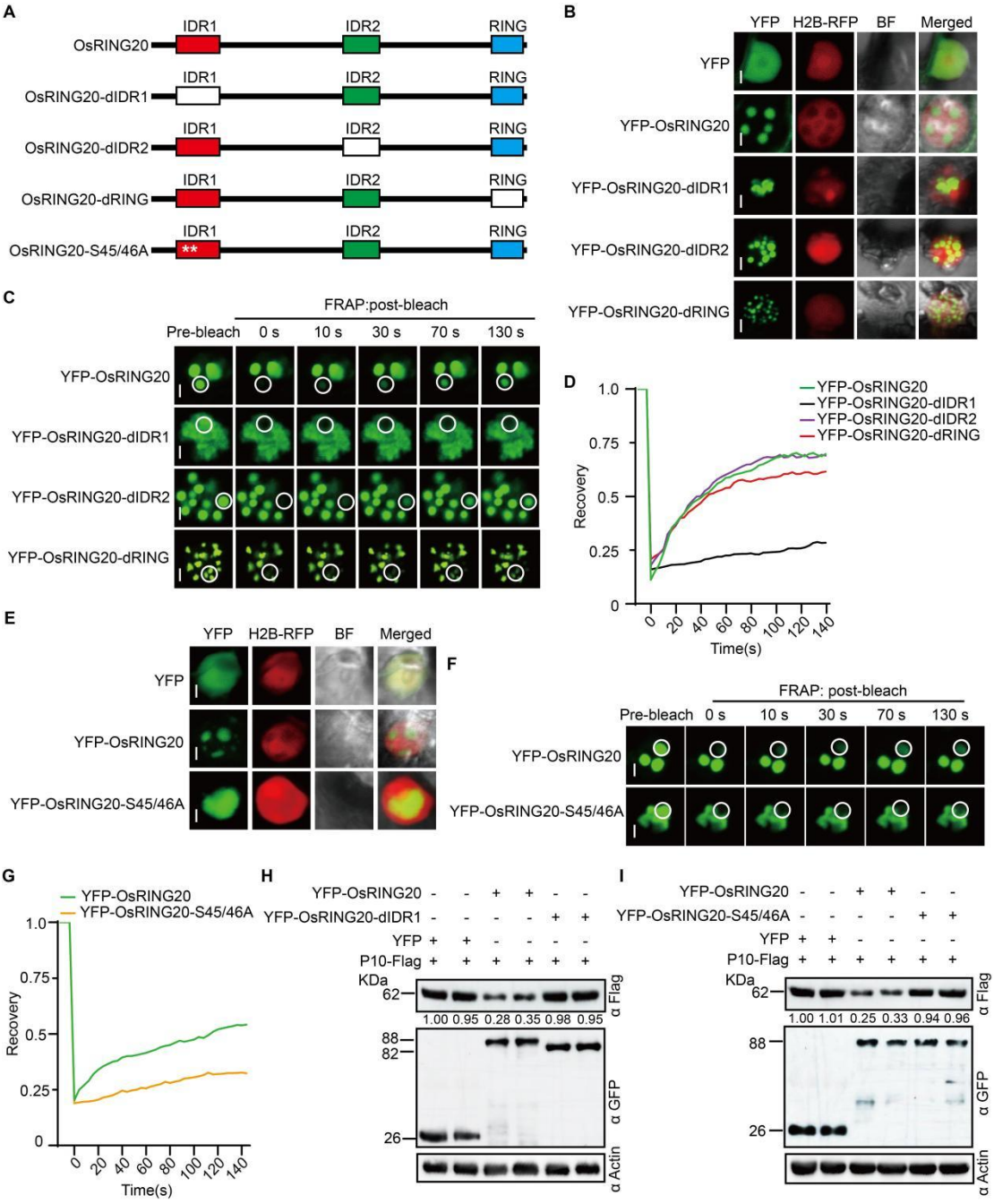

A
IDR1
IDR2
RING
OsRING20
OsRING20-dIDR1
OsRING20-dIDR2
OsRING20-dRING
OsRING20-S45/46A
**
B
YFP
H2B-RFP
BF
Merged
YFP
YFP-OsRING20
YFP-OsRING20-dIDR1
YFP-OsRING20-dIDR2
YFP-OsRING20-dRING
C
FRAP:post-bleach
Pre-bleach
0 s
10 s
30 s
70 s
130 s
YFP-OsRING20
YFP-OsRING20-dIDR1
YFP-OsRING20-dIDR2
YFP-OsRING20-dRING
D
YFP-OsRING20
YFP-OsRING20-dIDR1
YFP-OsRING20-dIDR2
YFP-OsRING20-dRING
Recovery
Time(s)
E
YFP
H2B-RFP
BF
Merged
YFP
YFP-OsRING20
YFP-OsRING20-S45/46A
F
FRAP: post-bleach
Pre-bleach
0 s
10 s
30 s
70 s
130 s
YFP-OsRING20
YFP-OsRING20-S45/46A
G
YFP-OsRING20
YFP-OsRING20-S45/46A
Recovery
Time(s)
H
YFP-OsRING20
YFP-OsRING20-dIDR1
YFP
P10-Flag
KDa
62
1.00 0.95 0.28 0.35 0.98 0.95
α Flag
88
82
26
α GFP
α Actin
I
YFP-OsRING20
YFP-OsRING20-S45/46A
YFP
P10-Flag
KDa
62
1.00 1.01 0.25 0.33 0.94 0.96
α Flag
88
26
α GFP
α Actin

Fig. 7

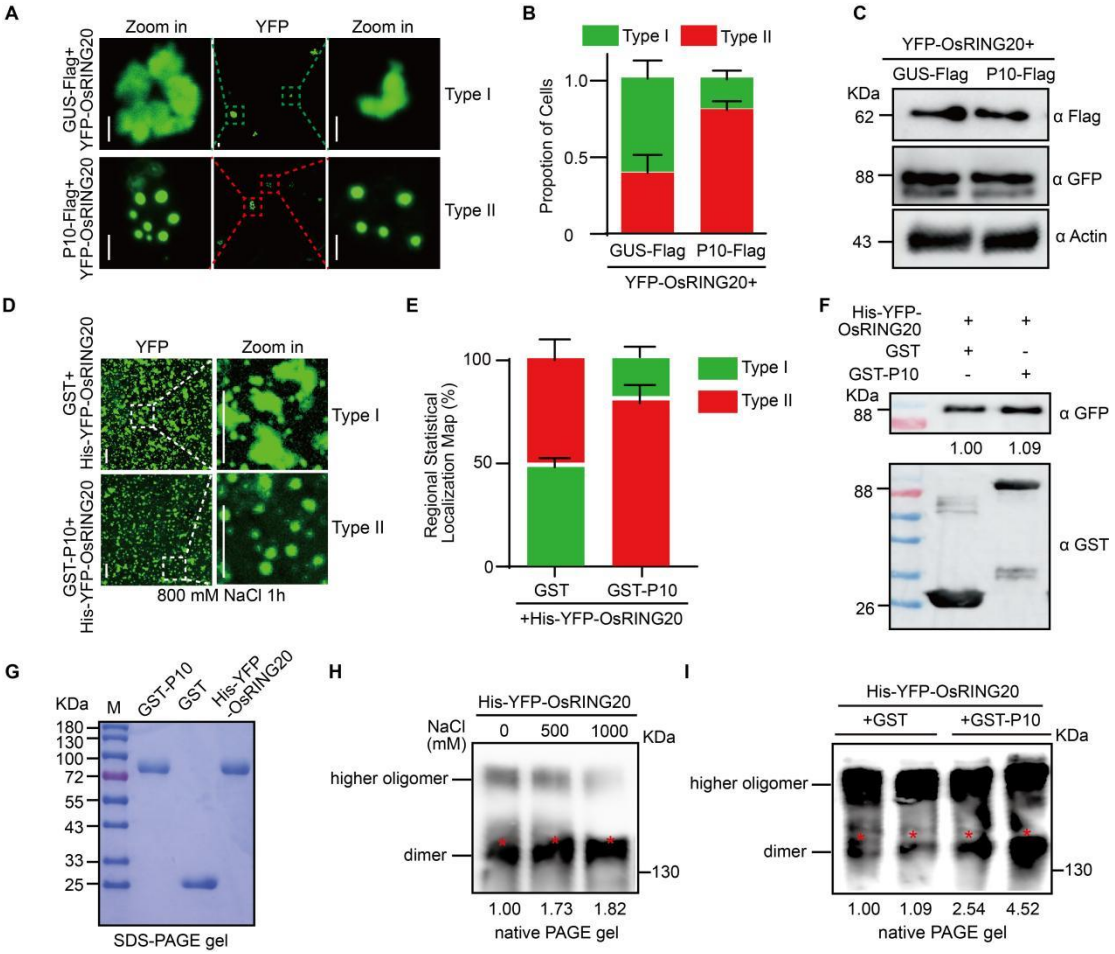

A
Zoom in
YFP
Zoom in
GUS-Flag+ YFP-OsRING20
P10-Flag+ YFP-OsRING20
Type I
Type II
B
Type I
Type II
Propotion of Cells
1.0
0.5
0
GUS-Flag
P10-Flag
YFP-OsRING20+
C
YFP-OsRING20+
GUS-Flag
P10-Flag
KDa
62
88
43
α Flag
α GFP
α Actin
D
YFP
Zoom in
GST+ His-YFP-OsRING20
GST-P10+ His-YFP-OsRING20
Type I
Type II
800 mM NaCl 1h
E
Regional Statistical Localization Map (%)
100
50
0
Type I
Type II
GST
GST-P10
+His-YFP-OsRING20
F
His-YFP-OsRING20
GST
GST-P10
KDa
88
α GFP
1.00
1.09
88
26
α GST
G
KDa
M
GST-P10
GST
His-YFP -OsRING20
180
130
100
72
55
43
33
25
SDS-PAGE gel
H
His-YFP-OsRING20
NaCl (mM)
0
500
1000
KDa
higher oligomer
dimer
130
1.00
1.73
1.82
native PAGE gel
I
His-YFP-OsRING20
+GST
+GST-P10
KDa
higher oligomer
dimer
130
1.00
1.09
2.54
4.52
native PAGE gel

Fig. 8

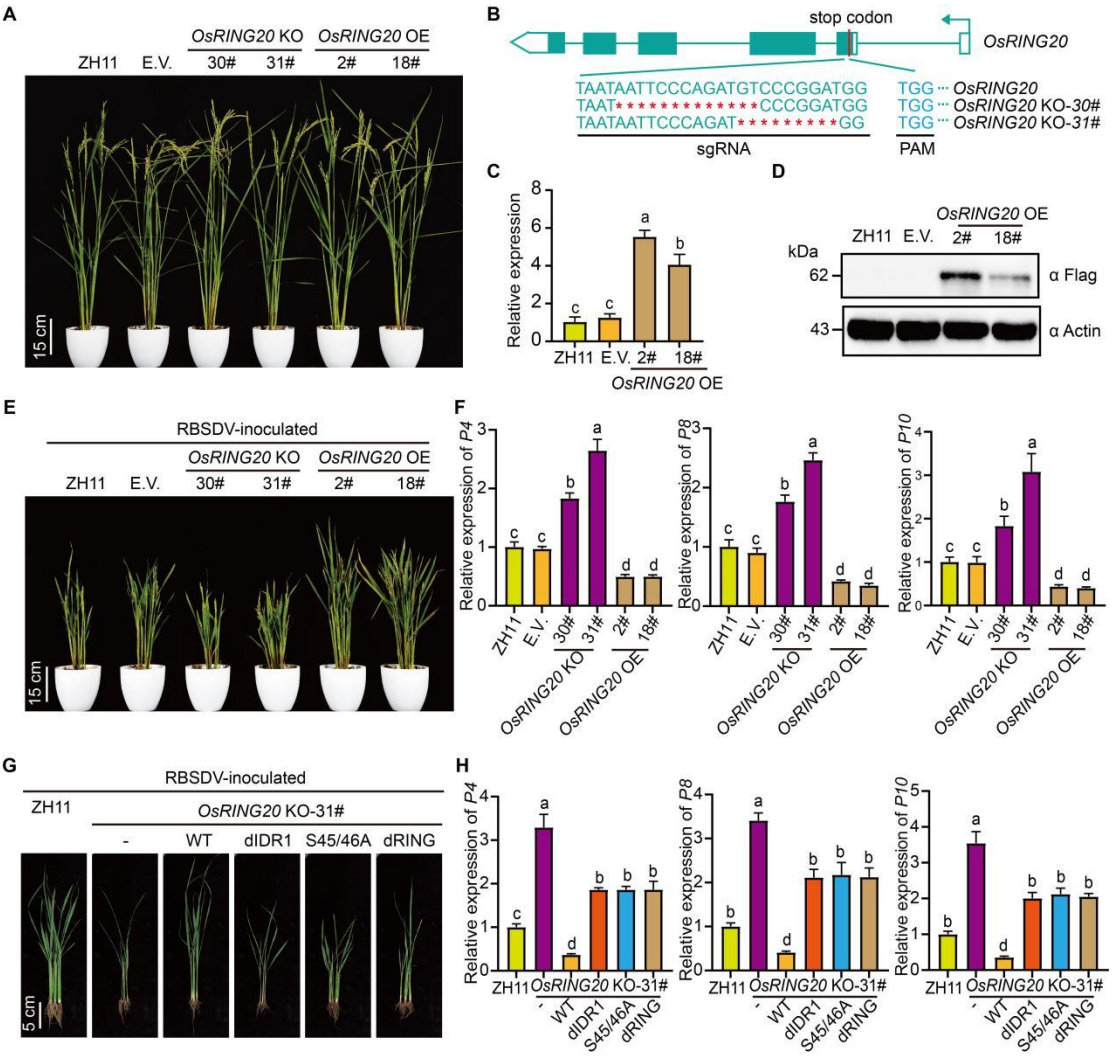

A
ZH11
E.V.
OsRING20 KO
30#
31#
OsRING20 OE
2#
18#
15 cm
B
stop codon
OsRING20
TAATAATTCCCAGATGTCCCGGATGG
TAAT**********CCCGGATGG
TAATAATTCCCAGAT*********GG
sgRNA
TGG ··· OsRING20
TGG ··· OsRING20 KO-30#
TGG ··· OsRING20 KO-31#
PAM
C
Relative expression
OsRING20 OE
D
kDa
62
43
α Flag
α Actin
E
RBSDV-inoculated
F
Relative expression of P4
Relative expression of P8
Relative expression of P10
G
OsRING20 KO-31#
-
WT
dIDR1
S45/46A
dRING
5 cm
H

Fig. 9

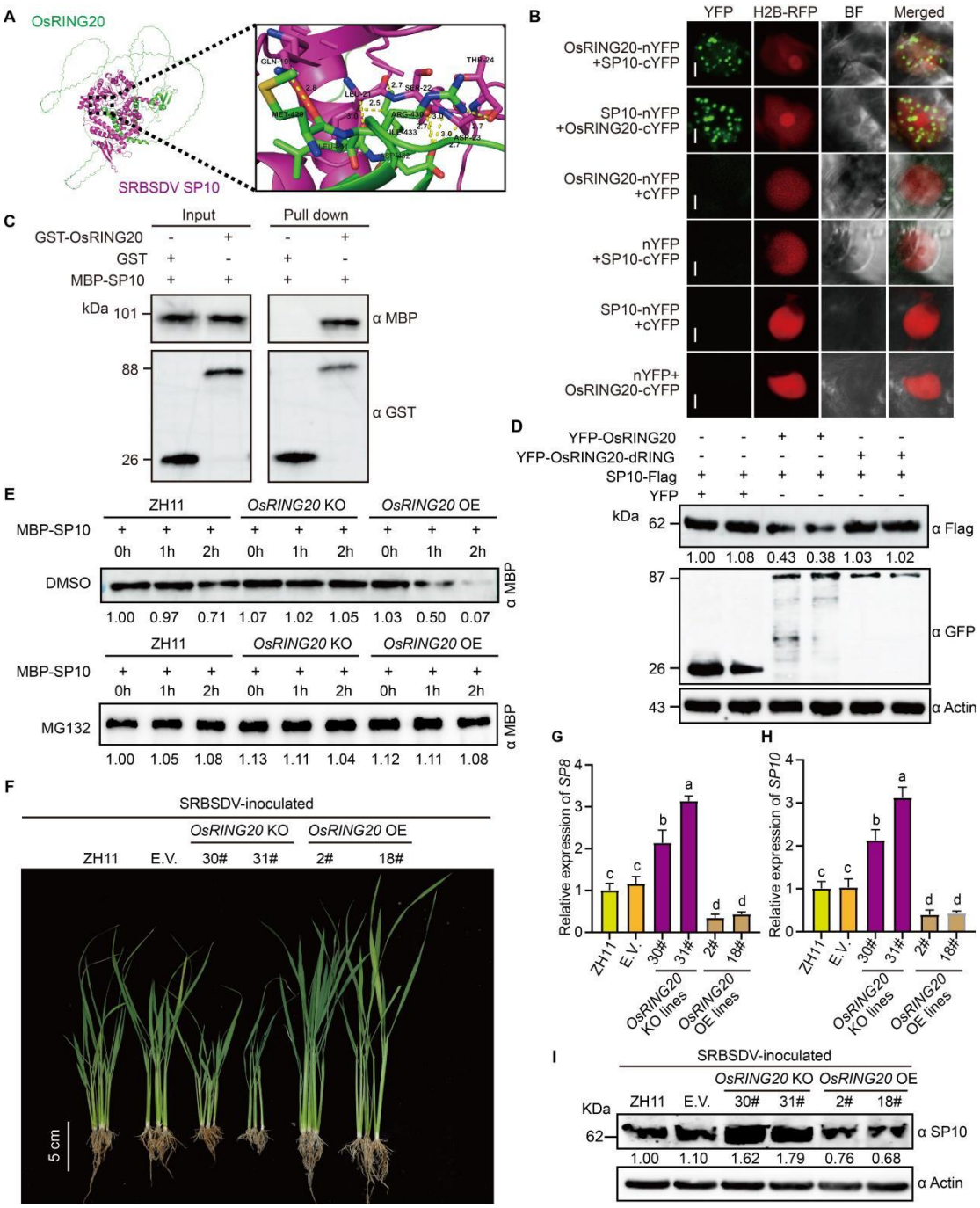
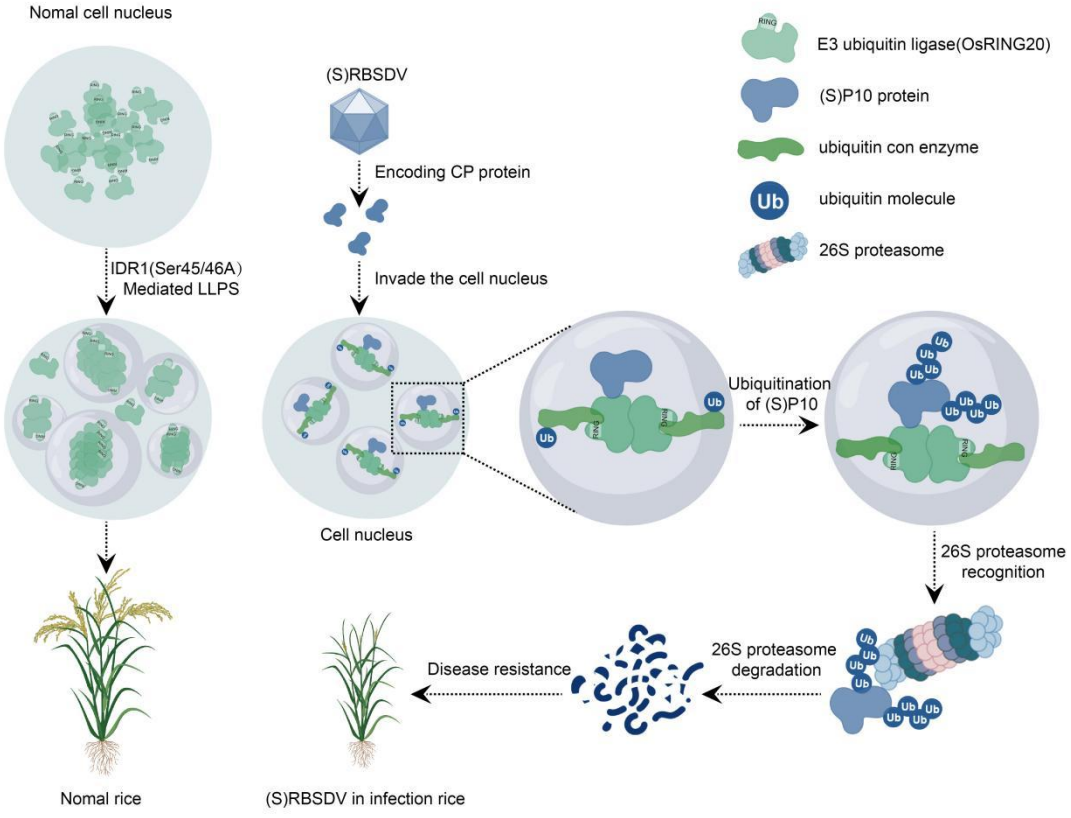

A
OsRING20
SRBSDV SP10
B
YFP
H2B-RFP
BF
Merged
OsRING20-nYFP +SP10-cYFP
SP10-nYFP +OsRING20-cYFP
OsRING20-nYFP +cYFP
nYFP +SP10-cYFP
SP10-nYFP +cYFP
nYFP+ OsRING20-cYFP
C
Input
Pull down
GST-OsRING20
GST
MBP-SP10
kDa
101
88
26
α MBP
α GST
D
YFP-OsRING20
YFP-OsRING20-dRING
SP10-Flag
YFP
kDa
62
α Flag
1.00 1.08 0.43 0.38 1.03 1.02
87
26
α GFP
43
α Actin
E
ZH11
OsRING20 KO
OsRING20 OE
MBP-SP10
0h 1h 2h 0h 1h 2h 0h 1h 2h
DMSO
α MBP
1.00 0.97 0.71 1.07 1.02 1.05 1.03 0.50 0.07
MG132
1.00 1.05 1.08 1.13 1.11 1.04 1.12 1.11 1.08
F
SRBSDV-inoculated
ZH11
E.V.
30#
31#
2#
18#
5 cm
G
Relative expression of SP8
ZH11
E.V.
OsRING20 KO lines
OsRING20 OE lines
H
Relative expression of SP10
I
SRBSDV-inoculated
KDa
62
α SP10
1.00 1.10 1.62 1.79 0.76 0.68
α Actin

Fig. 10


Nomal cell nucleus
(S)RBSDV
Encoding CP protein
Invade the cell nucleus
IDR1(Ser45/46A)
Mediated LLPS
Cell nucleus
E3 ubiquitin ligase(OsRING20)
(S)P10 protein
ubiquitin con enzyme
ubiquitin molecule
26S proteasome
Ubiquitination
of (S)P10
26S proteasome
recognition
26S proteasome
degradation
Disease resistance
Nomal rice
(S)RBSDV in infection rice

1209

Supplementary Files

This is a list of supplementary files associated with this preprint. Click to download.

- Supplementarymaterials.docx
- SupplementarymaterialsfulluncroppedGelsandBlotsimage.pdf